OUKA
The University of Osaka
Institutional Knowledge Archive

Title	Device Structure Design for Improving Color Purity in Light-Emitting Diodes Using Multinary Compound Semiconductor Quantum Dots
Author(s)	本村, 玄一
Citation	大阪大学, 2023, 博士論文
Version Type	VoR
URL	https://doi.org/10.18910/92930
rights	
Note	

The University of Osaka Institutional Knowledge Archive : OUKA

https://ir.library.osaka-u.ac.jp/

The University of Osaka

Doctoral Dissertation

Device Structure Design for Improving Color Purity in Light-Emitting Diodes Using Multinary Compound Semiconductor Quantum Dots

（多元化合物半導体量子ドットを用いた発光ダイオードの

色純度向上に向けたデバイス構造設計）

Genichi Motomura

June 2023

Department of Applied Chemistry

Graduate School of Engineering,

Osaka University

Preface

The studies presented in this thesis were conducted between 2016 and 2023 as a collaborative work between NHK Science & Technology Research Laboratories (STRL), Nagoya University, and Osaka University. The research was carried out under the guidance of Professor Dr. Susumu Kuwabata at Department of Applied Chemistry, Graduate School of Engineering, Osaka University.

The objective of this research is to design device structures that can enhance the luminescence characteristics of multinary compound semiconductor QDs, composed of elements from groups 11, 13, and 16. Additionally, the aim is to develop QD-LEDs with exceptional color purity, enabling the creation of vibrant light-emitting devices for displays.

The author holds a strong conviction that the findings obtained in this study will significantly contribute to the advancement of diverse display technologies, particularly in terms of achieving outstanding color reproduction, by utilizing QDs.

Genichi Motomura

Department of Applied Chemistry,
Graduate School of Engineering,
Osaka University
Suita, Osaka, Japan

June 2023

List of Publications

1. Efficient Quantum-Dot Light-Emitting Diodes using ZnS−$AgInS_2$ Solid-Solution Quantum Dots in Combination with Organic Charge-Transport Materials.
   Genichi Motomura, Kei Ogura, Tatsuya Kameyama, Tsukasa Torimoto, Taro Uematsu, Susumu Kuwabata, and Toshimitsu Tsuzuki
   Appl. Phys. Lett. **2020**, *116*, 093302. DOI: 10.1063/1.5143618

2. Electroluminescence from Band-Edge-Emitting $AgInS_2/GaS_x$ Core/shell Quantum Dots.
   Genichi Motomura, Kei Ogura, Yukiko Iwasaki, Taro Uematsu, Susumu Kuwabata, Tatsuya Kameyama, Tsukasa Torimoto, and Toshimitsu Tsuzuki
   Appl. Phys. Lett. **2020**, *117*, 091101. DOI: 10.1063/5.0018132

3. Green Electroluminescence Generated by Band-Edge Transition in Ag-In-Ga-S/GaS_x Core/shell Quantum Dots.
   Genichi Motomura, Yukiko Iwasaki, Tatsuya Kameyama, Tsukasa Torimoto, Taro Uematsu, Susumu Kuwabata, and Toshimitsu Tsuzuki
   ITE Trans. on MTA **2021**, *9*, 222−227. DOI: 10.3169/mta.9.222

4. Quantum-Dot Light-Emitting Diodes Exhibiting Narrow-Spectrum Green Electroluminescence by Using Ag−In−Ga−S/GaS_x Quantum Dots.
   Genichi Motomura, Taro Uematsu, Susumu Kuwabata, Tatsuya Kameyama, Tsukasa Torimoto, and Toshimitsu Tsuzuki
   ACS Appl. Mater. Interfaces **2023**, *15*, 6 8336−8344. DOI: 10.1021/acsami.2c21232

Contents

General Introduction *1*

Application of quantum dots (QDs) for wide color gamut display **1**
Quantum-dot light-emitting diodes (QD-LEDs) **3**
QD materials for QD-LEDs **4**
Multinary QDs with high color purity **6**
Present work **9**

Chapter 1 ..... *13*

1-1. Introduction **13**
1-2. Experimental section **15**
1-2-1. Synthesis of ZAIS QDs 15
1-2-2. Fabrication of ZAIS QD-LEDs 15
1-2-3. Characterization 17
1-3. Results and discussion **18**
1-3-1. PL characteristics of ZAIS QDs and EL spectra of ZAIS QD-LEDs 18
1-3-2. Layer separation of mixed EML in QD-LEDs 19
1-3-3. Improvement of EL characteristics of ZAIS QD-LEDs using CTMs 20
1-4. Summary **24**

Chapter 2 ..... *25*

2-1. Introduction **25**
2-2. Experimental section **27**
2-2-1. Synthesis of AIS core/shell QDs 27
2-2-2. Fabrication of AIS QD-LEDs 27
2-2-3. Characterization 28
2-3. Results and discussion **30**
2-3-1. PL characteristics of AIS core/shell QDs 30
2-3-2. EL spectra from AIS core/shell QDs including defect emission 31
2-3-3. Suppression of defect emission by mixing CTMs 32
2-3-4. EL characteristics of AIS QD-LEDs 33
2-4. Summary **36**

Chapter 3 ..... *37*

3-1. Introduction **37**
3-2. Experimental section **40**

3-2-1. Synthesis of AIGS core/shell QDs 40
3-2-2. Fabrication of AIGS QD-LEDs 40
3-2-3. Characterization 41
3-3. Results and discussion 43
3-3-1. PL characteristics of AIGS core/shell QDs 43
3-3-2. Improvement for mixed EML 44
3-3-3. $GaCl_3$ treatment of ZnMgO EIL 48
3-3-4. Application of highly transportable CTMs to QD-LEDs 49
3-4. Summary 53
Conclusions 55
References 57
Acknowledgements 64

General Introduction

Application of quantum dots (QDs) for wide color gamut display

Ultra-high-definition television (UHDTV) systems have been developed to provide realistic visual experiences that make viewers feel like they are present at the scene.[1] The UHDTV video format, defined by the International Telecommunication Union Radiocommunication sector (ITU-R) recommendation BT.2020,[2] specifies a wide color gamut that can express a wider range of colors than a conventional high-definition television (HDTV), which was defined by the ITU-R recommendation BT.709. The color gamut of the BT.2020 and BT.709 color spaces, represented with a CIE xy chromaticity diagram, are shown in Figure I. However, this wide color gamut exceeds the color range of current flat-panel displays, such as liquid crystal displays (LCDs) and organic light-emitting diode (OLED) displays. To achieve the wide color gamut of UHDTV, red, green, and blue primary colors with extremely high color purity are required.[3]

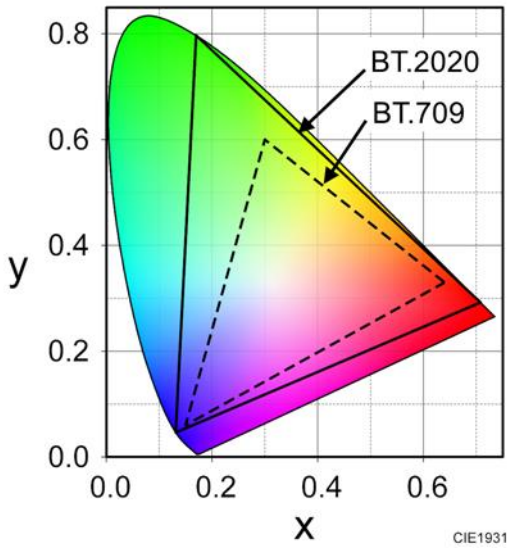


Figure I. Color gamut of the BT.2020 and BT.709 color space represented with a CIE xy chromaticity diagram. The outer solid triangle is the BT.2020 color gamut.

Quantum dots (QDs) are semiconductor nanocrystals with optical band gaps that can be controlled by their size, as shown in Figure II-a.[4-5] By controlling the size and composition of the QDs, it is possible to emit narrow-band, high-purity light over a wide range of wavelengths, from the visible to the near-infrared. This makes QDs attractive candidates for light-emitting elements in wide-color-gamut displays. Colloidal QDs are a type of QD that has a core of compound semiconductor nanocrystals synthesized in a liquid phase. A schematic image of core/shell QDs is shown in Figure II-b. The core emits light, and the surrounding organic ligands prevent the aggregation of the particles and allow dispersion of the QDs in a solvent. A core/shell structure is often used, in which the core surface is protected by a semiconductor shell with a band gap larger than that of the core material.[6]

There are two main approaches to using QDs in displays. The first is to use a blue light source and a QD filter to convert the light into red and green.[7-10] The second is to use red, green, and blue QD light-emitting diodes (QD-LEDs).[11-15] QD-LEDs can be used to create wide-

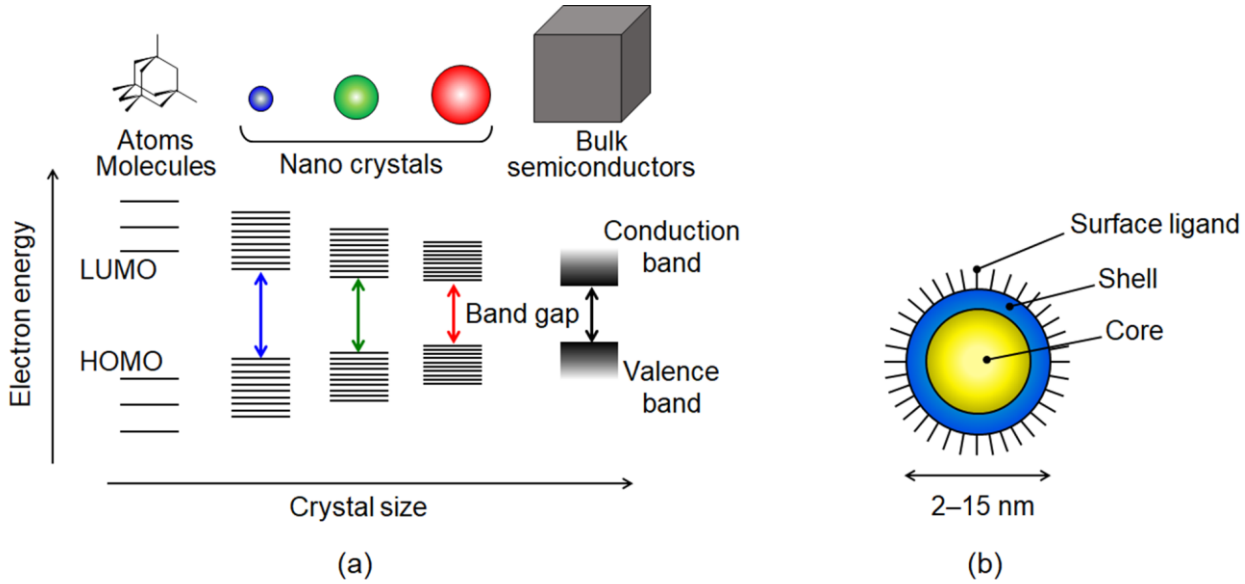


Figure II. (a) Schematic illustration of energy band gap tuning of QDs by their crystal size, and (b) Schematic illustration of colloidal core/shell QD stabilized by organic ligands.

gamut, high-quality displays. They can also be manufactured using coating and printing processes, making them suitable for large-screen displays and low-cost applications.[16-17] QDs are a promising technology for displays, and they have the potential to enhance the visual experience.

Quantum-dot light-emitting diodes (QD-LEDs)

The electroluminescence (EL) properties of QD-LEDs have also been studied.[11-15] QD-LEDs, which are fabricated using a thin film of QDs as the emitting layer (EML), have a structure similar to that of organic LEDs (OLEDs). A typical QD-LED has a structure consisting of anode, hole injection layer (HIL), hole transport layer (HTL), QD EML, electron transport layer (ETL), electron injection layer (EIL), and cathode on a substrate, as shown in Figure III. When an electric current is passed through the device, electrons and holes are injected into the QDs, generating excitons, which are pairs of an electron and a hole. These

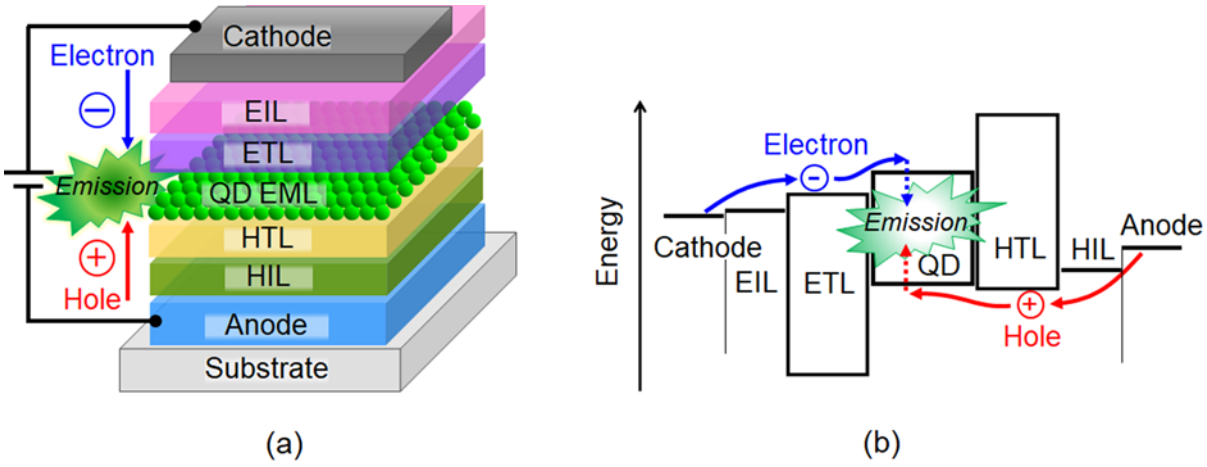


Figure III. (a) Schematic illustration of device structure for typical QD-LEDs, and (b) energy diagram of typical QD-LEDs.

excitons recombine and release energy in the form of light. The color of the emitted light can be precisely controlled by adjusting the size or composition of the QDs.

In order to enhance the performance of QD-LEDs, it is crucial to not only improve the luminescence properties of the QDs themselves, but also to achieve a proper balance of injected electrons and holes within the QDs to generate excitons and facilitate light emission. To fully exploit the luminescence capabilities of QDs, it is essential to carefully design the device structure and ensure that the fabrication processes are capable of producing the intended design.

QD-LEDs can be applied not only to full-color flat panel displays but also to flexible, large-scale, and high-resolution displays.[18-19] Ongoing research and development efforts continue to improve the efficiency, color accuracy, and scalability of QD-LEDs, making them a promising technology for future-generation displays.

QD materials for QD-LEDs

A comparison of typical QD materials used in QD-LEDs is shown in Table I. Cadmium compounds are typical materials for QDs, and several QD-LEDs based on CdSe QDs have been reported. It was first reported that the color of QD-LEDs based on CdSe can be varied by changing the size of the nanoparticles (NPs).[11] Since 2010, the luminous efficiency of QD-LEDs has rapidly improved. [20-23] A red QD-LED with an external quantum efficiency (EQE) of 20%, comparable to that of organic LEDs, has been reported.[24] The efficiency and lifetime of QD-LEDs of various colors, including green and blue, have been further improved.[25-30]

Table I. Comparison of typical QD materials used in QD-LEDs.

	Cd compound QDs	InP-based QDs	ZnSe-based QDs	Multinary compound semiconductor QDs
Core	CdSe, CdS	InP	ZnSe, ZnSeTe	$AgInS_2$, $CuInS_2$
Shell	CdS、ZnSe、ZnS	ZnSe、ZnS	ZnS	ZnS, GaS_x
Color	R, G, B	R, G	B	R, G, B
Color purity	Excellent	Good	Good	Defect emission: Poor Band-edge emission: Very good
Luminous efficiency	Excellent	Good	Good	Fair (under development)

However, the toxicity of Cd is a major impediment to its practical use, as it is a heavy metal that can have harmful effects on the environment.

Numerous materials have been investigated as low-toxicity QDs for use in QD-LEDs. Indium phosphide (InP) is a group III–V semiconductor, and InP QDs are a promising substitute for Cd-based QDs.[31-32] InP-based QDs require precise control of their particle size and are likely to have defects on their surface or at the core/shell interface. These defects can lead to reduced light emission and color purity. Therefore, achieving a high luminous efficiency and color purity with InP QDs is more difficult than with Cd-based QDs. InP QDs with improved light-emission characteristics can be achieved by carefully controlling their particle size, shell structure, and composition.[33-36] This could lead to the development of InP-based LEDs with high luminous efficiency and color purity, which would be a valuable alternative to Cd-based LEDs. Advances in device structure and QD structure have led to improved performance of QD-LEDs fabricated using InP-based QDs.[37-41] A green QD-LED based on InP/ZnSeS QDs with an EQE of 3.46%[42] and a red QD-LED based on InP/ZnSe/ZnS QDs with an EQE of 6.6%[43] have been reported. The efficiency has since been further improved, and red QD-LEDs with EQEs greater than 20% have been reported.[44]

ZnSe-based QDs are promising candidates for blue emission, and highly efficient blue QD-LEDs have been reported. ZnSe QDs have a direct band gap, which makes them suitable for emission in the blue region.[45-46] In addition, ZnSe QDs can be synthesized with high uniformity and narrow size distributions. ZnSe QDs are considered for doping with Te to achieve a redshift in luminescence, thereby obtaining a vibrant blue emission.[47-50] However, it is difficult to maintain a sharp spectrum when the emission is redshifted by doping with Te.[51]

Multinary compound semiconductor QDs (multinary QDs), composed of elements from groups 11, 13, and 16, such as $AgInS_2$ (AIS) [52] and $CuInS_2$ (CIS) [53-55], have attracted considerable attention in the field of photofunctional devices. Compared to binary QDs, multinary QDs offer distinct advantages, including greater compositional flexibility for precise band gap tuning than conventional binary QDs. For instance, by introducing ZnS or substituting Ag with Cu, In with Ga, and S with Se, the PL of $AgInS_2$ QDs can be effectively shifted to the visible and near-infrared regions. [56-59] In terms of color purity, multinary QDs exhibit an emission with a full width at half maximum (FWHM) in the range of 100–200 nm, which is significantly broader than that of II−VI (20–30 nm) and III−V (35–60 nm) QDs, primarily due to their emission originating from lattice defect sites. QD-LEDs utilizing $AgInS_2$-based and $CuInS_2$-based QDs have demonstrated broad EL spectra originating from the intrinsic defect levels in the QDs. Despite some applications utilizing these broad spectra for white emission, they remain unsuitable for high color purity requirements.[60-61]

Multinary QDs with high color purity

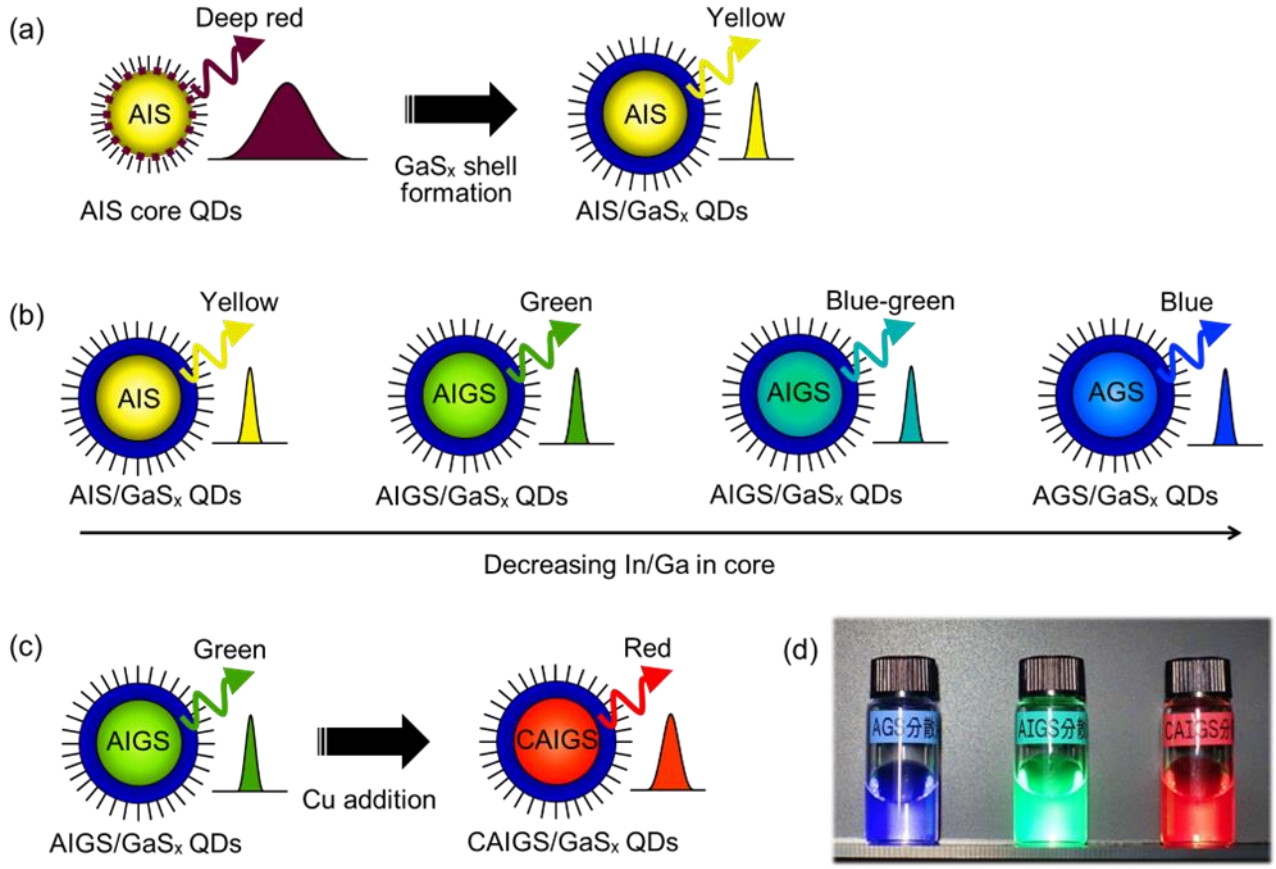


Figure IV. Schematic illustrations of material improvement for high color purity and multi-color of multinary QDs. (a) Formation of GaS_x shell on the AIS core QDs significantly enhances the intensity and narrows the PL peak. (b) Emission from the AIS core/shell QDs can be blue shifted by increasing Ga ratio. (c) Addition of Cu to AIGS core/shell QDs red shift the emission. (d) Photograph of multinary QDs emitting in three primary colors.

In recent studies, $AgInS_2$-based QDs have been found to exhibit intense and spectrally narrow PL from band-edge transitions. While $AgInS_2$ core QDs show a broad PL peak, the introduction of a GaS_x shell onto the core structure, forming $AgInS_2/GaS_x$ core/shell QDs (AIS core/shell QDs), results in a highly intense and narrow PL peak (Figure IV-a).[62] This improvement can be attributed to the effective passivation of numerous surface defects on the core particles by the GaS_x shell. Unlike the commonly used ZnS shell, which fails to passivate

defect sites on $AgInS_2$ cores, the GaS_x shell successfully protected the core surface and demonstrated a defect-free core/shell interface.

Furthermore, the use of Ag–In–Ga–S/GaS_x core/shell QDs (AIGS core/shell QDs) composed of solid-solution NPs of Ag–In–S and Ag–Ga–S with a GaS_x shell has demonstrated tunable band-edge emission within the visible light region (Figure IV-b).[63] The brightness and vividness of the green luminescence in AIGS core/shell QDs were improved by using highly reactive raw materials and optimizing the synthesis procedures. [64-66] Notably, the AIGS core/shell QDs exhibited a sufficiently narrow FWHM of 31 nm, which distinguishes them from other Cd-free QDs.[67] AIGS core/shell QDs can also emit blue light at shorter wavelengths by further increasing the Ga ratio, and red light at longer wavelengths by adding Cu or Se (Figure IV-c).[68-69] The realization of multi-color QDs with three primary colors (red, green, and blue) makes them promising as full-color light-emitting materials with high color purity (Figure IV-d).

Present work

This study aims to design a device structure that enhances the EL properties of QD-LEDs using multinary QDs composed of elements from groups 11, 13, and 16. The primary goal is to develop QD-LEDs with high color purity by utilizing core/shell QDs based on AIS (AIGS) materials. Previous research on multinary QDs has successfully achieved QDs that exhibit high color purity emissions originating from band-edge transitions. However, realizing the high color purity in QD-LEDs requires efficient extraction of the luminescence properties of the QDs as thin films and precise control of the charge injection process.

The presence of crystal defects in multinary QDs can degrade color purity by introducing broad emission components. Therefore, it is essential to suppress the emission associated with these defects in order to achieve high color purity in EL. To address these challenges, the focus was on optimizing the device structure by combining QDs with organic charge transport materials (CTMs). It is noteworthy that phase separation of the QDs and CTMs occurs gradually during coating process. The substantial CTM layer promotes charge injection into the QD layer while preventing leakage of the opposite charge. It was observed that the mixed EML not only improves the transport properties of the EML but also suppresses defect emission components. The optimization of the device structure, coupled with the improvements in the luminescence properties of multinary QDs, has facilitated the successful development of QD-LEDs utilizing green multinary QDs. This breakthrough has led to the generation of green EL with exceptionally high color purity. The achievement of such high color purity green light emission in QD-LEDs using multinary QDs is a significant progress in the field, and is expected to lead to the realization of displays with a wide color gamut.

Chapter 1 describes novel type of QD-LEDs that utilizes a combination of ZnS-$AgInS_2$ (ZAIS) QDs, denoted as $(AgIn)_xZn_{2(1-x)}S_2$, and organic CTMs.[70] Although ZAIS QDs exhibit broadband defect emission, they emit light with a high quantum yield without the need for a core/shell structure, making them ideal for investigating the introduction of organic CTMs. This discussion focuses on exploring the combination of ZAIS QDs with organic CTMs, as well as describing the impact of these materials on the transport properties and enhancement of luminous efficiency.

The QD-LEDs were fabricated using ZAIS QDs. These QDs exhibit red photoluminescence, with a peak wavelength of approximately 700 nm. Due to the relatively low charge-injection barrier of ZAIS QDs lacking a wide-band-gap shell, the QD-LEDs employ red ZAIS QDs in conjunction with organic CTMs to facilitate electron injection from an organic ETL. The resulting QD-LEDs demonstrate an EQE of 2.2%, a turn-on voltage of 2.4 V, and emit red light with chromaticity coordinates of (0.66, 0.33).

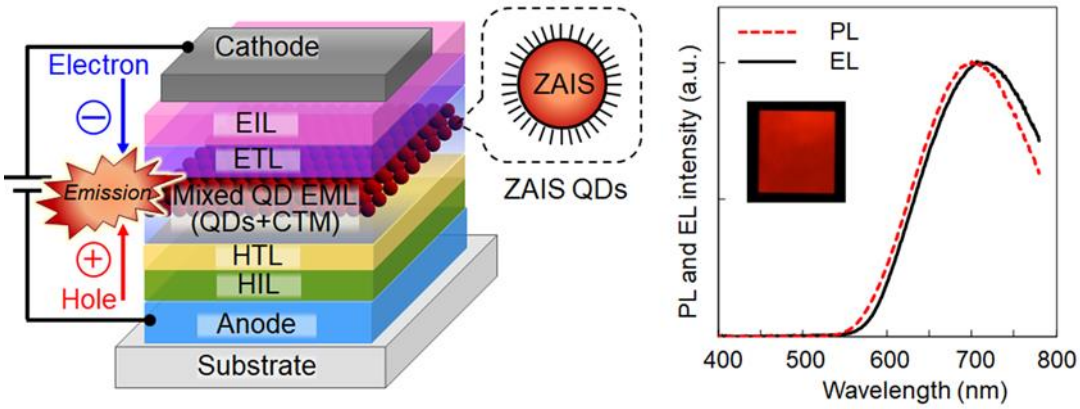


Figure V. Device structure and emission spectra of QD-LEDs using ZAIS QDs, as described in Chapter 1.

Chapter 2 describes the EL spectral analysis of QD-LEDs using AIS core/shell QDs.[71] These QDs exhibit a remarkably high color purity yellow emission attributed to band-edge transitions. However, the experiments revealed that there is an increase in EL-specific defect emission, which consequently resulted in a deterioration of color purity. To address this issue, the implementation of an EML composed of a mixture of QDs and CTMs was explored aiming to suppress the defect emission components.

The defect emission is considered to occur due to the electrons flowing within the EML being easily trapped at defect sites of the QDs. The addition of CTMs as electron transporters in the EML yielded effective suppression of defect emission, reaching a level comparable to that observed in the PL spectrum of the AIS core/shell QD film. The introduction of CTMs demonstrated an improvement in electron injection into the QDs and facilitated a better balance of carriers within the EML.

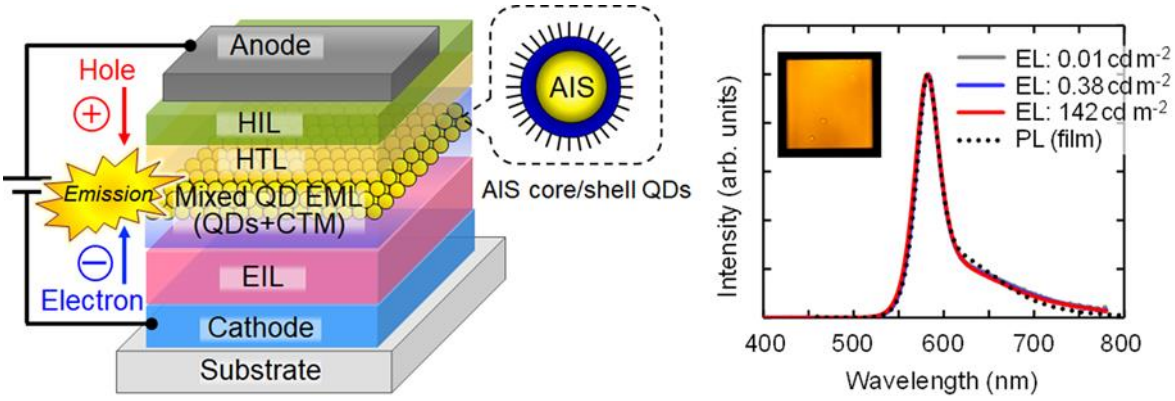


Figure VI. Device structure and emission spectra of QD-LEDs using AIS core/shell QDs, as described in Chapter 2.

Chapter 3 describes the development of QD-LEDs that showcase green EL utilizing AIGS core/shell QDs.[72-73] This chapter shows the process of enhancing the color purity of the green ELs through further improvements to the AIS-based QD-LEDs discussed in Chapter 2.

The EL spectra obtained from the AIGS QD-LEDs exhibited a significant defect emission component, to the extent that the intensity of defect emission surpassed that of the band-edge emission. This defect emission was larger than the corresponding component of the AIS QD-LEDs, which emit yellow, and was not completely suppressed by mixing CTMs. The origin of this defect emission was attributed to electrons injected into the EML, which tended to be trapped at defect sites within the QDs. Ga compounds were introduced into both the EML and the EIL, which effectively compensated for the defect sites on the QD surface and prevented electron injection into these defect sites. In addition, the luminescence properties of the QD-LEDs were further optimized by selecting CTMs with excellent transport properties.

As a result, the defect emission components in the EL were successfully suppressed. The QD-LEDs exhibited EL spectra with a remarkably sharp FWHM of 30 nm, which is an exceptional feature for a low-toxicity QD.

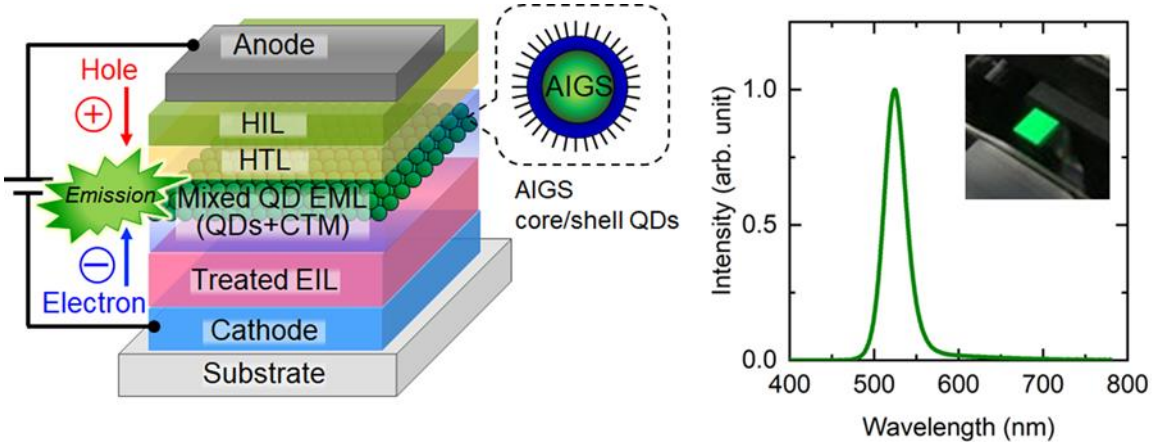


Figure VII. Device structure and emission spectra of QD-LEDs using AIGS core/shell QDs, as described in Chapter 3.

Chapter 1

QD-LEDs using ZnS−$AgInS_2$ QDs in Combination with Organic Charge-Transport Materials

1-1. Introduction

Multinary QDs in the groups 11, 13, and 16 without coating by GaS_x shell generally emit defect emission with a broad spectral width. The ZAIS QDs used in this chapter were suitable for use in QD-LEDs because their optical properties and electronic energy levels could be controlled as functions of two parameters: particle size and chemical composition.[74] The peak wavelength of the PL of the ZAIS QDs was controllable within a wide range from 530 to 810 nm by changing the fraction of ZnS content in the ZAIS as well as by particle-size control, and their PL quantum yield (QY) was sufficiently high for them to be used in LEDs. For instance, ZAIS QDs that emit red PL showed a PLQY of 79%. They exhibit high PLQY as core-only QDs that do not require a shell. The shell covering the surface of QDs is formed by a semiconductor with a large band gap, which is a factor that prevents charge injection into QDs. ZAIS QDs, which do not require a shell, are expected to be suitable for charge injection devices.

With respect to the application of multinary QDs with defect emission to QD-LEDs, Tan *et al.* observed electroluminescence from QDs consisting of $CuInS_2$–ZnS alloy cores (ZCIS) and ZnSe/ZnS shells. EL emission peaked at red, yellow, and green wavelengths was observed from the QD-LEDs containing ZCIS/ZnSe/ZnS core/shell QDs of 2.3 nm, 2.7 nm, and 3.3 nm-diameters, respectively.[57] Bhaumik *et al.* reported QD-LEDs based on Zn-alloyed $AgInS_2$ QDs combined with ZnO NPs deposited on top of the QD layer as an electron-transporting material. These QD-LEDs exhibited EL, but their EQEs remained as low as 0.02%.[75] Zhu *et al.* reported inverted QD-LEDs with Zn–Ag–In–

S QDs as emissive layers. QD-LEDs with a stepwise HTL and ZnO NPs as an ETL exhibited a low turn-on voltage of 2.2 V, a high luminance exceeding 2000 cd m^{-2}, and an efficiency of 2.1 cd A^{-1}.[76] Kim *et al.* reported the synthesis of core/shell Cu–In–S (CIS)/ZnS QDs and the fabrication of highly efficient QD-LEDs, which exhibited yellow emission with an EQE as high as 7.3%.[77] All of these QD-LEDs had a common feature in that ZnO NPs were used as the ETL.

In chapter 1, the fabrication of QD-LEDs using ZAIS QDs as low-toxicity QDs was reported, and the effects of organic CTMs on the EL properties from the viewpoint of charge injection into the QDs were discussed. The ZAIS QD-LEDs fabricated using 2,2′,2″-(1,3,5-benzinetriyl)-tris(1-phenyl-1H-benzimidazole) (TPBi) as the ETL exhibited greater efficiency than ZAIS QD-LEDs fabricated using ZnO NPs as the ETL.[78] Moreover, a higher efficiency and lower turn-on voltage were achieved by mixing CTMs into the EML.

1-2. Experimental section

1-2-1. Synthesis of ZAIS QDs

ZAIS QDs with the composition $(AgIn)_xZn_{2(1-x)}S_2$ (x = 0.2, 0.4, and 0.8) were synthesized according to a previously reported method.[74] Here, the QDs synthesized with x = 0.8 were mainly used. Powders of $Ag(CH_3COO)$, $In(CH_3COO)_3$, and $Zn(CH_3COO)_2 \cdot 2H_2O$ with a mole ratio of 0.8:0.8:0.4 (total metal ions: 0.20 mmol) were added to a test tube containing thiourea powder (0.20 mmol). After 3.0 mL of oleylamine/1-dodecanthiol mixed solvent was added and the precursor powders were completely dissolved, the solution was heated to 250 °C for 10 min with vigorous stirring under a N_2 atmosphere. The obtained solution was cooled to room temperature, and then large particles were removed from the solution by centrifugation. ZAIS QDs were isolated from the supernatant by precipitation induced by the addition of methanol. The wet precipitates were dissolved in n-hexane. The ZAIS QDs were then washed three times by the addition of ethanol before being dispersed in toluene.

1-2-2. Fabrication of ZAIS QD-LEDs

Figure 1-1-a shows the device structures of the QD-LEDs fabricated using the red-emitting ZAIS, and Figure 1-1-b shows a transmission electron microscopy (TEM) image of the ZAIS QDs as well as the chemical structures of the organic materials used in the devices.

Indium tin oxide (ITO)-coated glass substrates were rinsed and degreased by sequential sonication in a detergent solution, water, and ethanol, followed by further treatment using a UV–ozone cleaner immediately before the substrates were used. First, a hole injection layer (HIL) of poly(3,4-ethylenedioxythiophene): poly(styrenesulfonic acid) (PEDOT:PSS, P AI4083, Clevios) was spin-coated at 2500 rpm onto the ITO glass substrate and baked at 180 °C for 60 min. A HTL composed

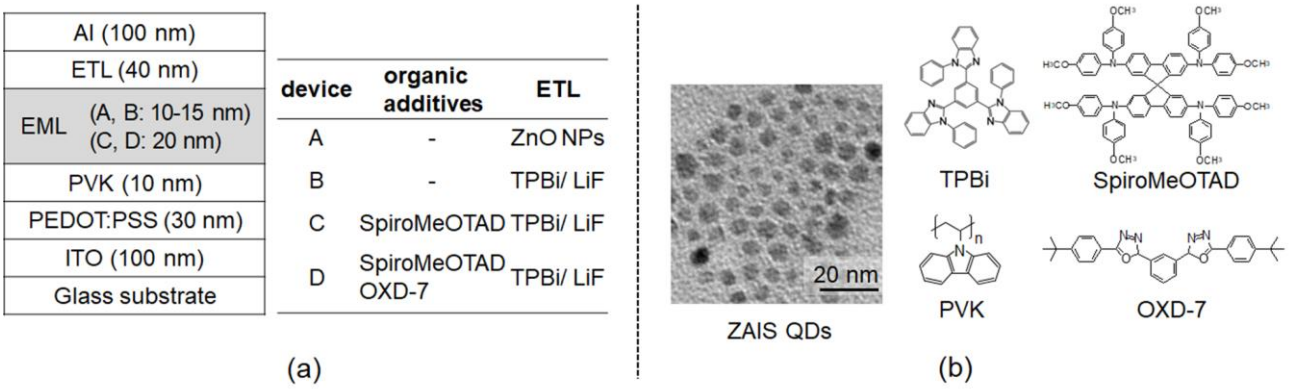


Figure 1-1. (a) Structure of QD-LEDs fabricated using red-emitting ZAIS and the layer conditions of each device and (b) representative TEM image of ZAIS QDs and the chemical structures of the organic materials in them.

of poly(*N*-vinylcarbazole) (PVK, Acros Organics) was spin-coated from 1,2-dichloroethane solution (4 mg mL^{-1}) at 2000 rpm on top of the HIL and baked at 150 °C for 30 min under a N_2 atmosphere. The thickness of the PVK layer after film formation was 20 nm.

In the subsequent coating of the emitting layer (EML), part of the PVK layer was dissolved in toluene and its thickness was reduced to 10 nm. Toluene solutions of the ZAIS QDs (6 mg mL^{-1}) were prepared for depositing EMLs for each device; the ZAIS QDs were used in their as-deposited form for devices A and B. For device C, 2,2′,7,7′-tetrakis[*N*,*N*-di(4-methoxyphenyl)amino]-9,9′-spirobifluorene (SpiroMeOTAD, 3 mg mL^{-1}) was added to the QD solution; for device D, SpiroMeOTAD and 1,3-bis[2-(4-*tert*-butylphenyl)-1,3,4-oxadiazo-5-yl]benzene (OXD-7) were added (SpiroMeOTAD: 2.1 mg mL^{-1}; OXD-7: 0.9 mg mL^{-1}) to the QD solution. These EMLs of the ZAIS QDs were spin-coated at 2000 rpm and baked at 100 °C for 30 min under a N_2 atmosphere. The EML thickness of devices A and B, where the EMLs were formed only by QDs, was 10–15 nm; that of devices C and D, where the EMLs included one or two organic additives, was ~20 nm.

For device A, on top of the ZAIS layer, ZnO NPs were spin-coated from a 1-butanol dispersion (20 mg mL^{-1}), which was prepared in accordance with a previously reported method,[22] and the ETL with

a thickness of 40 nm was deposited. The substrates were then loaded into a vacuum deposition chamber. On top of the EMLs of devices B, C, and D, a 40 nm-thick ETL consisting of TPBi, a 1 nm-thick electron-injecting layer of LiF, and 100 nm-thick anode of Al were successively deposited by vacuum evaporation at 1×10^{-4} Pa. The devices were encapsulated with a glass cap under a N_2 atmosphere.

1-2-3. Characterization

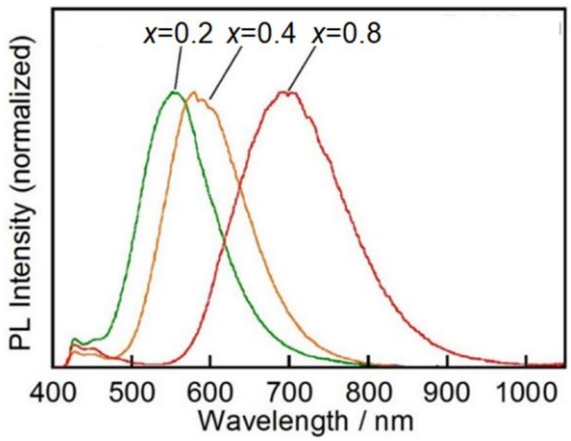
The PL spectra of the materials in the QD-LEDs were recorded with a spectrofluorometer (HORIBA FluoroMax-4). The current–voltage characteristics of the devices were measured using a source meter (Keithley 2400), their luminance was measured using a luminance meter (KonicaMinolta LS-110), and their EL spectra were recorded using a spectroradiometer (Konica Minolta CS-1000). The EQE was calculated from the luminance, current density, and EL spectrum under the assumption of Lambertian emission.

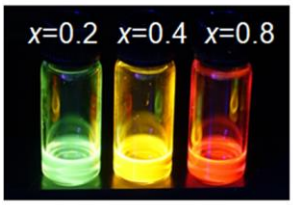
1-3. Results and discussion

1-3-1. PL characteristics of ZAIS QDs and EL spectra of ZAIS QD-LEDs

Figure 1-2 shows PL characteristics of ZAIS QD dispersion: ZAIS QDs with compositions of $(AgIn)_xZn_{2(1-x)}S_2$ (x = 0.2, 0.4, 0.8) were synthesized. The toluene dispersion of ZAIS QDs exhibited red, green, and red PL, with a peak wavelength of 550 nm, 590 nm, and 700 nm, respectively. The red ZAIS QDs, which were synthesized at x = 0.8, were found to have a high PL quantum yield of 86%.

The fabricated ZAIS QD-LEDs of the devices A–D emitted red light with approximately similar EL spectra when a DC voltage was applied between the cathode and anode. Figure 1-3-a shows the EL spectrum of device D was selected as a representative spectrum for all of the devices; the PL spectrum of ZAIS QD dispersion after purification are shown for comparison. The PL and EL spectra show broad peaks, which were assignable to defect-site emission of the ZAIS. The FWHM values of the EL spectra of devices A–D were equally 170 nm, and the peak wavelength varied slightly in the range from 695 to 710 nm depending on the device structure. Although the ZAIS QDs exhibited broad





x	Peak (nm)	PL QY (%)
0.2	550	40
0.4	590	72
0.8	700	86

Figure 1-2. PL characteristics of ZAIS QD dispersion: ZAIS QDs with compositions of $(AgIn)_xZn_{2(1-x)}S_2$ (x = 0.2, 0.4, 0.8) were synthesized.

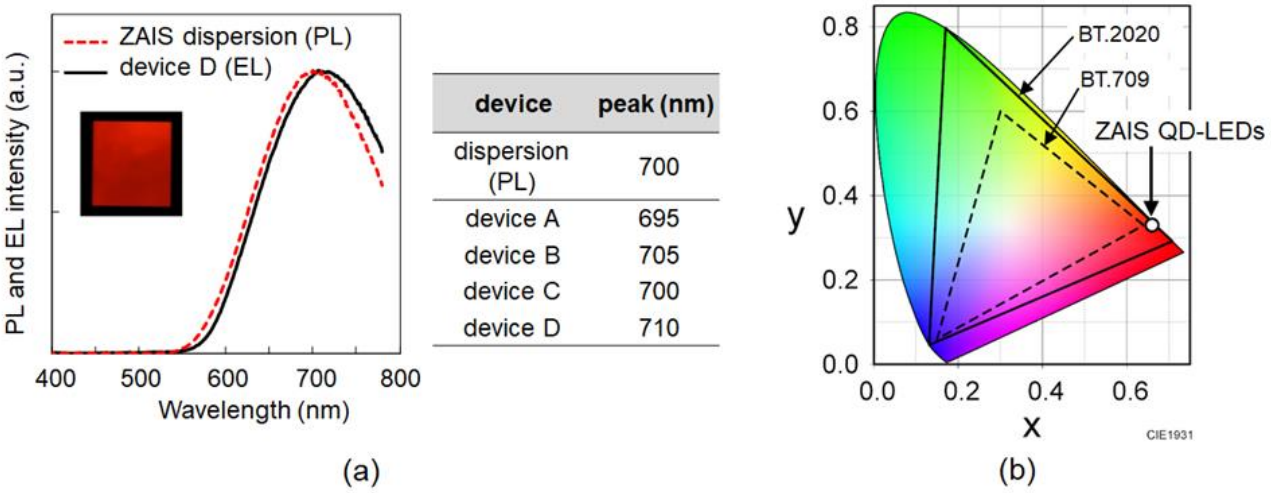


Figure 1-3. (a) EL spectrum of device D and PL spectrum of ZAIS dispersed after purification. The peak wavelength of each device is shown in the table. (b) Chromaticity of ZAIS QD-LEDs in CIE xy chromaticity diagram.

emission spectra, the EL emission exhibited a good red color with chromaticity coordinates (0.66, 0.33) because of the use of long-wavelength QDs (Figure 1-3-b).

1-3-2. Layer separation of mixed EML in QD-LEDs

Figure 1-4 shows a cross-sectional scanning transmission electron microscopy (STEM) image of a QD-LED with the same structure as device D. Each layer can be distinguished, revealing that an appropriate layered structure was obtained. However, ZAIS QDs and organic CTMs were not

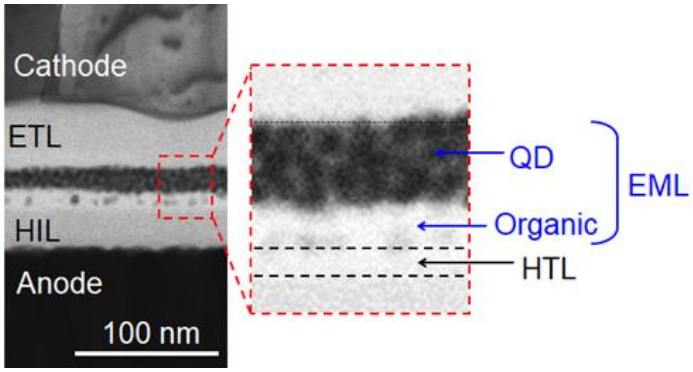


Figure 1-4. Cross-sectional STEM image of a QD-LED with the same structure as device D and an enlarged view of the EML.

uniformly dispersed in the EML. The QDs were covered with an alkyl chain, which has a low surface energy,[79] and polar molecules tended to phase-separate when the solvent was dried during the coating process.[80] Depending on the combination of materials and the coating conditions, QDs were able to be reproducibly deposited onto the top of the EML, while CTMs settles at the bottom.[39-40, 81] The phase separation conditions could be realized repeatedly by washing the QDs carefully and quickly drying them during spin-coating. Most of the ZAIS QDs were located at the ETL side of the EML, leaving organic CTMs at the HTL side. The mixed CTMs were composed mainly of SpiroMeOTAD, a hole-transport material, in order to properly inject electrons and holes into ZAIS QDs. The fact that individual QDs with high electron density can be seen in the STEM image suggest that some CTMs are incorporated in the gaps between the QDs.

1-3-3. Improvement of EL characteristics of ZAIS QD-LEDs using CTMs

I here discuss the results associated with improving the EL characteristics in progressive stages from device A to device D. The devices were adjusted for charge balance, focusing on electron injection into the EML and charge transport in the EML. Figure 1-5 shows (a) the

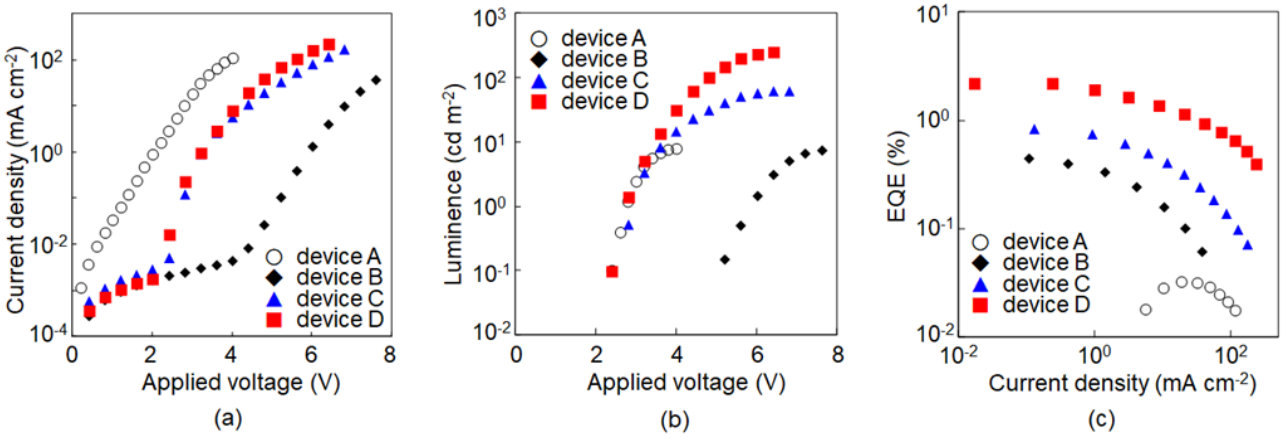


Figure 1-5. Plots of (a) current density–applied voltage, (b) luminance–applied voltage, and (c) EQE–current density for devices A–D.

applied voltage–current density, (b) the applied voltage–luminance, and (c) the current density–EQE characteristics of devices A, B, C, and D.

The current density of device A was much higher than those of devices B, C, and D. The ZnO NPs used as the ETL in device A exhibited high electron mobility (μ_e = 1.3 × 10^{-3} cm^2 V^{-1} s^{-1}) were suitable for electron transport from the Al cathode and excellent electron injection properties for QD layers.[21] The turn-on voltage for emission was approximately 2.4 V for device A, whereas the maximum EQE was as low as 0.03%. In this device, the balance of holes and electrons in the EML was poor and excess electrons passed through the counter electrode. From the viewpoint of electron injection and hole confinement in the QD layer, the ETL adjacent to the QD layer should have a high lowest unoccupied molecular orbital (LUMO) level and a low highest occupied molecular orbital (HOMO) level. Figure 1-6 also shows the energy levels of each material used in the QD-LEDs. The conduction-band energy (E_{CB}) and valence-band energy (E_{VB}) levels for the ZAIS QDs[74] and ZnO NPs[22] and the HOMO–LUMO energy levels for each organic layer were taken from the literature.[82-84] Although ZnO NPs have a wide band gap, they are not sufficiently hole-blocking due to the presence of many defect levels.

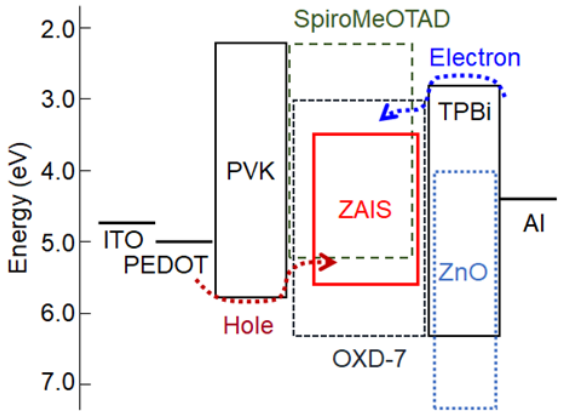


Figure 1-6. Energy levels of the materials used in the QD-LEDs.

On the contrary, the energy levels of the edges of the conduction band and valence band of the ZAIS QDs have been estimated to be 3.4 eV and 5.4 eV, respectively. The charge injection barrier of the ZAIS QDs without a wide-bandgap shell is relatively low. Therefore, TPBi, which is an organic ETL, was used in device B instead of ZnO NPs. The EQE improved to 0.4% because of the suppression of excessive electron injection. However, device B, which was fabricated using a TPBi ETL, exhibited a higher driving voltage (turn-on voltage of 5.2 V) than device A, which was fabricated with a ZnO ETL.

Next, both improvement of the quantum efficiency and reduction of the driving voltage were attempted. The low conductivity between ZAIS QDs in the EML would also increase the driving voltage. To solve this problem, organic CTMs were added to the EML to improve its conductivity. Therefore, some of the organic additive molecules were located between the ZAIS QDs and enhanced the transportability of the EML. Only SpiroMeOTAD was added to the QD layer for device C to improve hole mobility, whereas both SpiroMeOTAD and OXD-7 were added to the QD layer for device D to improve both the electron mobilities and the hole mobilities.

The current density of devices C and D containing SpiroMeOTAD was higher than that of device B. The turn-on voltage for emission for devices C and D was approximately 2.4 V, which was the same as that for device A; by contrast, that for device B was 5.2 V. This difference is attributed to SpiroMeOTAD penetrating between the ZAIS QDs and enhancing hole transport in the EML.

Device D, which had both electron- and hole-transport materials in its EML, exhibited further improved characteristics. The addition of SpiroMeOTAD and OXD-7 improved the

balance of holes and electrons in the EML, and an EQE as high as 2.2% was recorded for red-emitting devices fabricated using ZAIS QDs. A high efficiency and low driving voltage were achieved for the QD-LEDs prepared using the combination of ZAIS and organic CTMs.

1-4. Summary

QD-LEDs using ZAIS as a low-toxicity QD were fabricated. Because the charge-injection barrier of ZAIS without a wide-bandgap shell is relatively low, the QD-LEDs with red ZAIS QDs in combination with organic CTMs can properly inject electrons from an organic ETL. The QD-LEDs exhibited an EQE of 2.2%, turn-on voltage of 2.4 V, and red emission with chromaticity coordinates (0.66, 0.33). The results indicate that ZAIS QDs can be used in combination with organic CTMs to improve the properties of QD-LEDs. The independent control of both particle size and chemical composition of ZAIS QDs will be advantageous in optimizing QD-LED performance. Multinary QDs, such as ZAIS, are candidates for a novel class of Cd-free QDs for QD-LEDs.

Chapter 2

Electroluminescence from Band-Edge-Emitting $AgInS_2/GaS_x$ Core/shell QDs

2-1. Introduction

Recently, I–III–VI-based multinary QDs have been reported to generate intense, spectrally narrow PL from a band-edge transition.[62, 85] Whereas AIS core QDs exhibited a broad PL peak, AIS core/shell QDs covered with GaS_x shells exhibited an intense narrow PL peak at 585 nm with an FWHM of 30 nm and a significantly high PLQY of 56%. AIS core/shell QDs exceed InP-based QDs in terms of narrow spectra and have potential as low-toxicity QDs with high color purity. In order to apply these narrow-spectra emission to QD-LEDs, the Els in multinary QDs were investigated.

To achieve the same luminescence in EL as in PL, it is crucial to control the process of injecting electrons and holes into the QD EML, enabling the proper generation of excitons and light emission. ZnO NPs are considered suitable as EILs in QD-LEDs because they exhibit excellent electron injection into the QDs.[86] However, the presence of defect sites in ZnO NPs makes excitons easily transferred or quenched by an interfacial charge transfer process at the ZnO/QD interface, so they must be used without increasing the new defect emission components.[87]

In the case of InP-based QD-LEDs, high color purity emission from QDs was achieved by employing a mixed EML consisting of QDs and CTMs in inverted structure QD-LEDs, in which ZnO NPs EIL is formed under the EML.[39-40] Based on the inverted structure, the EL

spectra of AIS QD-LEDs and the device structure to achieve the color purity of Els were investigated.

In chapter II, QD-LEDs using AIS core/shell QDs that exhibit the band-edge emission were fabricated and their EL properties were investigated. Whereas the QD-LED with an EML consisting of only AIS core/shell QDs showed substantial, broad defect emission along with the sharp band-edge emission, the QD-LEDs with an EML consisting of AIS core/shell QDs mixed with CTMs with electron transport properties exhibited sharp band-edge emission. The defect emission was suppressed to the same level as in the PL spectrum of the AIS core/shell QD film.

2-2. Experimental section

2-2-1. Synthesis of AIS core/shell QDs

The AIS core/shell QDs used as a light-emitting material were synthesized by the following method.[62, 85] For $AgInS_2$ core NPs, silver acetate (0.4 mmol) and indium acetate (0.4 mmol) were mixed with oleylamine (8 mL) and 1-dodecanethiol (1.25 mmol) under an Ar atmosphere; the temperature of the resultant mixture was then increased to approximately 80 °C. 1,3-dimethylthiourea was added; the temperature was then increased to 140 °C, maintained for 30 min to grow NPs, and then lowered to room temperature. The NPs were centrifuged to remove large particles, precipitated by the addition of excess methanol, and dispersed in chloroform. To achieve the surface-coated AIS core/shell QDs, approximately 30 nmol (in terms of NPs) of $AgInS_2$ core NPs were mixed with an oleylamine (7 mL) suspension containing gallium acetylacetonate (0.1 mmol) and 1,3-dimethylthiourea (0.1 mmol). The reaction mixture was heated to 280 °C under an Ar atmosphere and then cooled to room temperature in air. The AIS core/shell QDs were washed several times with methanol and ethanol and uniformly dissolved in chloroform.

2-2-2. Fabrication of AIS QD-LEDs

Figure 2-1 shows the structure of the QD-LED with an EML consisting of only the AIS core/shell QDs (a), shows the structure of the QD-LED with an EML composed of a mixture of AIS core/shell QDs and CTMs (b), and structure of AIS core/shell QDs and chemical structures of organic materials in them (c). Glass substrates on which a 100 nm-thick ITO cathode was patterned were rinsed and degreased by sequential sonication in a detergent solution and ethanol, followed by further treatment using a UV–ozone cleaner. A 40 nm-thick EIL of ZnO NPs were spin-coated from a 1-butanol

dispersion (20 mg mL^{-1}), which was prepared in accordance with a previously reported method,[22] under a N_2 atmosphere and baked at 180 °C for 30 min.

Here, the AIS core/shell QD concentration was fixed at 3 mg mL^{-1} in chloroform, and tris(2,4,6-trimethyl-3-(pyridin-3-yl)phenyl)borane (3TPYMB)[88] as CTMs was added to some of the dispersions. The QD:3TPYMB mixing ratios were 1:0 (no addition of 3TPYMB) and 1:0.5 by weight. The QD dispersions for EMLs were spin-coated onto the EIL, which was subsequently baked at 100 °C. This QD-LED had a QD EML approximately 10 nm thick and composed of two or three layers of QD particles. The substrates were then loaded into a vacuum deposition chamber, and a 40 nm-thick HTL consisting of tris(4-carbazoyl-9-ylphenyl) amine (TCTA), a 10 nm-thick HIL of MoO_3, and an 80 nm-thick anode of Al were successively deposited. The devices were encapsulated with a glass cap under a N_2 atmosphere.

2-2-3. Characterization

The PL spectra were recorded with a spectrofluorometer (HORIBA FluoroMax-4). The current–voltage characteristics were measured with a source meter (Keithley 2400). The luminance was

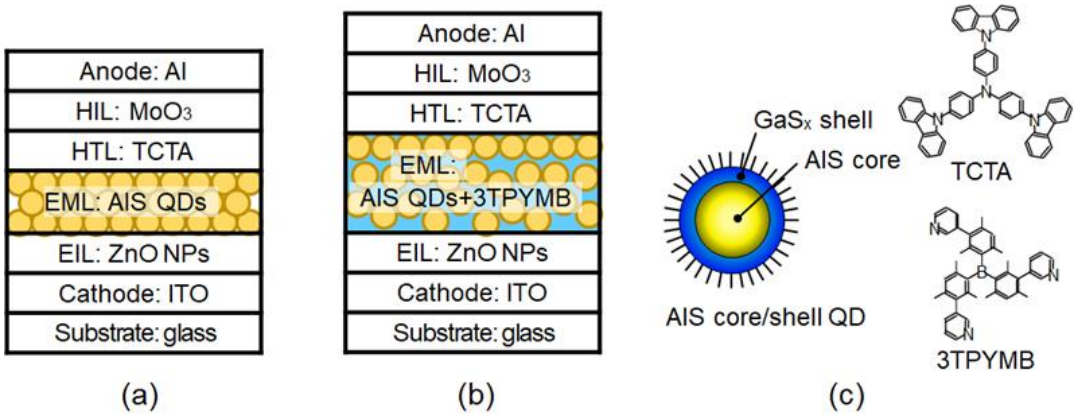


Figure 2-1. Structures of (a) an AIS QD-LED with an EML consisting of only QDs and (b) an AIS QD-LED with an EML containing QDs mixed with 3TPYMB. (c) Structure of AIS core/shell QDs and chemical structures of organic materials in QD-LEDs.

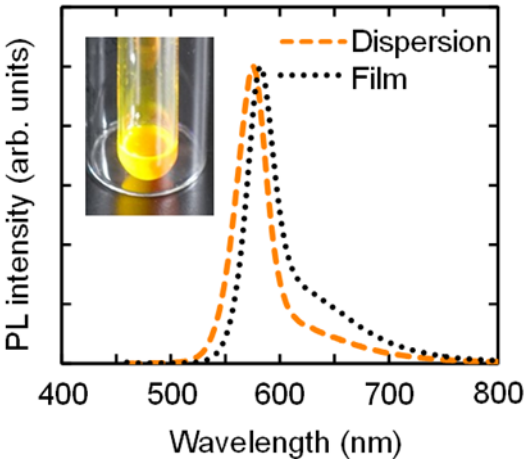
measured with a luminance meter (Konica Minolta LS-110). The EL spectra were recorded with a spectroradiometer (Konica Minolta CS-2000A). The EQE was calculated from the luminance, current density, and EL spectrum under the assumption of Lambertian emission. The thickness of the spin-coated films was measured with a stylus profiler (Bruker DektakXTL).

2-3. Results and discussion

2-3-1. PL characteristics of AIS core/shell QDs

Figure 2-2 shows the PL spectra normalized at the band-edge emission peak intensity of the synthesized AIS core/shell QDs as a dispersion in chloroform and as a spin-coated film. Figure 2-2 The AIS core/shell QD dispersion exhibited yellow PL with an intense sharp peak at a wavelength of approximately 575 nm and a broad shoulder in the wavelength range beyond 600 nm. the sharp peak derived from band-edge transition was obtained by suppressing surface defects of the AIS through formation of the GaS_x shell. The identification of the emission as the band-edge transition was judged from the wavelength of UV-vis absorption edge and the shorter PL decay lifetime than that of the defect emission.

The peak wavelength was 575 and 583 nm, the FWHM was 33 and 34 nm, and the PLQY was 70% and 31% for the AIS core/shell QDs dispersion and the film, respectively. These results confirm that the PL spectra of the AIS core/shell QD film tended to spread to the longer-wavelength side compared with the dispersion. It is considered that the excitation energy for the film is more easily transferred to QDs with defect sites which have lower energy levels.



	Peak (nm)	FWHM (nm)	PL QY (%)
Dispersion	575	33	70
Film	583	34	31

Figure 2-2. PL spectra of synthesized AIS core/shell QDs in chloroform and QD film and specific PL characteristics.

2-3-2. EL spectra from AIS core/shell QDs including defect emission

Figure 2-3-a shows the PL and EL spectra recorded under three luminance conditions of the AIS QD-LEDs; the intensity was normalized at the peak wavelength. The wavelength of the sharp band-edge emission for EL was approximately the same in the corresponding PL spectrum obtained by irradiating the emitting-layer film. However, the intensity of the sub-peak derived from defect emission was higher in the EL spectra than in the corresponding PL spectrum of the AIS core/shell QD film. The greater defect emission observed in the EL spectra than in the PL spectrum might be due to the different excitation mechanisms between them causing the transfer of a greater number of excitons than those photo-excited to the defect levels either directly or through bands.

In typical QD-LEDs, excitons of the QDs are generated by the injection of electrons and holes from electron/hole transport layers into the conduction/valence band of the QDs. The difference between EL and PL suggests the existence of specific defect sites on the incomplete shell surface and the degradation of the QD/electron injection layer interface (Figure 2-3-b). If such defect sites can more easily accept externally injected charges than their photogenerated counterparts, it would explain the

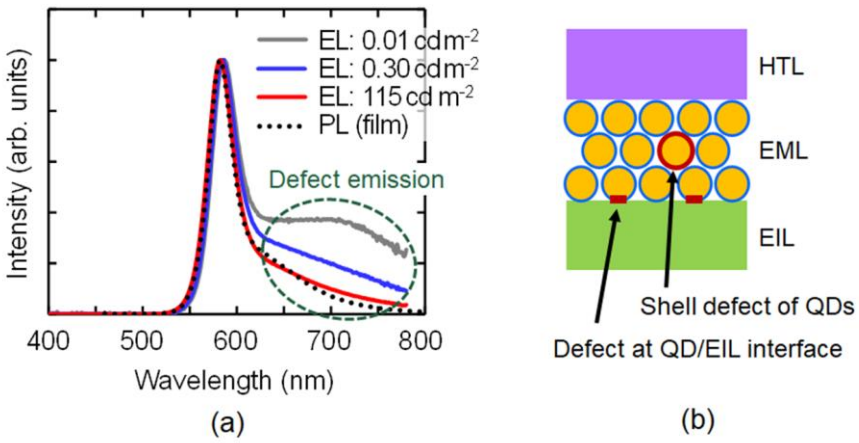


Figure 2-3. (a) EL spectra of AIS QD-LED depending on luminance and the PL spectrum and (b) defect factors in the QD emitting layer.

higher ratio of defect emission in the EL spectra. Therefore, the injected charges will fall into the defect levels of the QDs and the defect emission will tend to increase compared with the PL.

The increased defect emission at low luminance is explained as follows. The increase in band-edge emission purity may arise from the saturation of defect levels because the decay lifetime of the defect emission (~ 1 μs) was longer than that of the band-edge emission (~30 ns).[62] In addition, the probability of the carriers becoming trapped in the defect levels in the QD film would change depending on the electric field.[89] Thus, the improvement of the charge transport process in the QD film may lead to the suppression of the defect emission.

2-3-3. Suppression of defect emission by mixing CTMs

To further increase the purity of band-edge emission by changing charge injection conditions, 3TPYMB as CTMs was mixed with the QDs, which effectively suppressed defect emission in the EL spectra. The EMLs were spin-coated from chloroform solutions containing AIS core/shell QDs and 3TPYMB. Figure 2-4-a shows the PL and EL spectra recorded under three luminance conditions of the AIS QD-LEDs with 3TPYMB incorporated into the EML; the intensity was normalized at the

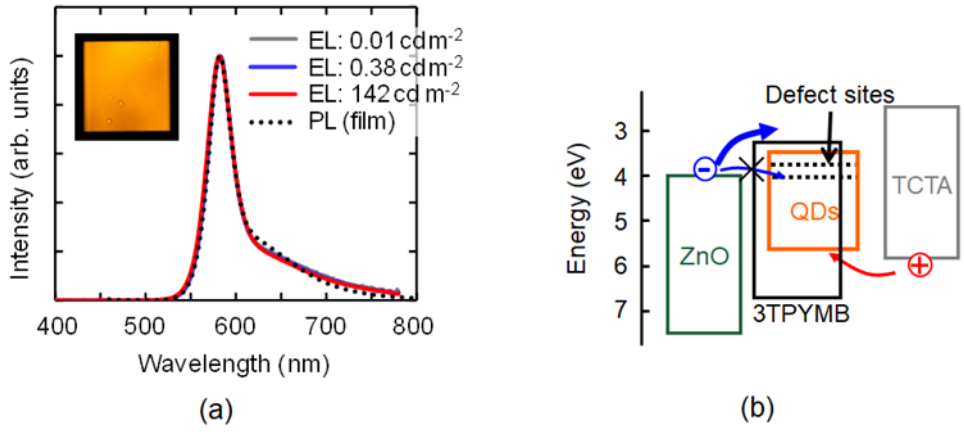


Figure 2-4. (a) EL spectra of the AIS QD-LED with 3TPYMB incorporated into the EML depending on luminance and the PL spectrum. (b) Energy levels of the materials used in AIS QD-LEDs.

peak wavelength. The inset photograph shows the yellow EL from the AIS QD-LEDs. The defect emission in the EL spectra under lower luminance conditions was found to be effectively suppressed. The defect emission was suppressed to the same level as that in the PL spectrum of the AIS core/shell QD film.

The mixed 3TPYMB effectively separated the QDs from the ZnO NPs, preventing direct electron injection into defect levels into the QDs. As a result, electrons injected into the EML were less likely to be trapped in defect levels, resulting in the suppression of defect emission. Fig. 4(b) shows the energy levels of the materials used in AIS QD-LEDs. The valence-band E_{VB} of the QDs was measured by photoelectron spectroscopy (AC-3), and the conduction-band E_{CB} was calculated from the E_{VB} and the band gap estimated from the energy at the absorption edge. The energy levels of the other materials were taken from the literature.[22, 88, 90] The LUMO of 3TPYMB is close to the E_{CB} of the QDs, indicating easy electron injection from 3TPYMB to the QDs. By contrast, holes are injected from TCTA into the QDs directly rather than through the HOMO of 3TPYMB because the HOMO level is more than 1 V lower than both the E_{VB} of the QDs and the HOMO of TCTA. In addition, the EL spectra that were hardly affected by the type of HTL indicate that most of the defect levels exist near the conduction-band edge of the AIS core/shell QDs.

2-3-4. EL characteristics of AIS QD-LEDs

The current density and luminance–applied voltage curves for the QD-LEDs in which 3TPYMB was incorporated into the EML are shown in Figure 2-5-a. The EQE–current density characteristics of the QD-LEDs fabricated with a 3TPYMB-mixed EML are shown in Figure 2-5-b. While mixing 3TPYMB increased the maximum luminance from 250 cd m^{-2} to 720 cd m^{-2}, an increase in the turn-

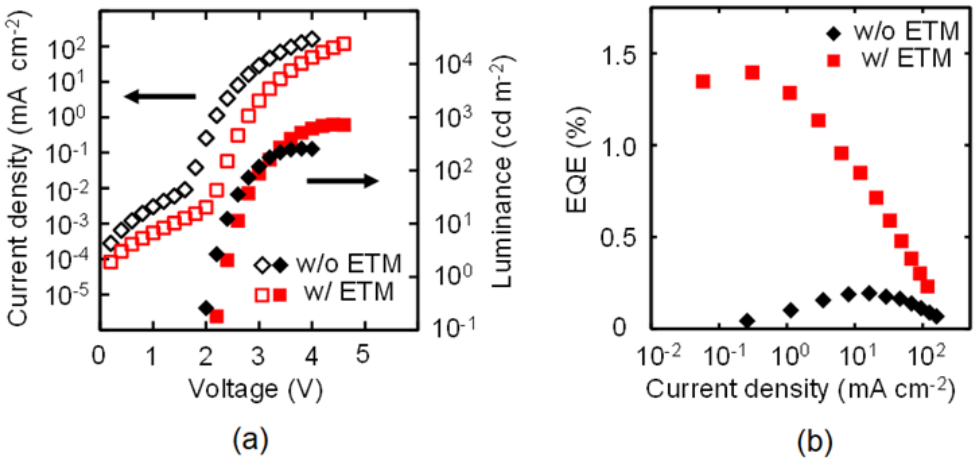


Figure 2-5. (a) Current density and luminance-applied voltage plots, and (b) EQE-current density plots for AIS QD-LEDs without and with 3TPYMB.

on voltage with mixing of 3TPYMB indicates that the electron injection through 3TPYMB is difficult compared with the direct injection from the ZnO EIL. The EQE values were improved by the incorporation of a small amount of 3TPYMB: from 0.2% in the absence of 3TPYMB to 1.4% in the device corresponding to a mixing ratio of 1:0.5.

For the device fabricated without 3TPYMB, the electrons that could not cross the injection barrier were more likely to be injected into the defect levels, resulting in defect emission and luminescence deactivation. However, when the QDs were embedded in 3TPYMB and the direct injection route for the electrons was blocked, the number of electrons trapped at the EIL–QD interface likely decreased. Therefore, the electrons were less likely to be trapped at the defect level, which led to not only suppression of the defect emission but also improvement of EQEs. This improvement is attributed to the hole-blocking property of 3TPYMB promoting balance between electrons and holes in the EML.

From these results, the addition of 3TPYMB was found to be beneficial with respect to the balance between reducing defect emission in the EL spectrum and maintaining the EL characteristics in the QD-LEDs. For further improvement of the EL characteristics, the GaS_x shell should be modified to improve the PLQY of the AIS core/shell QD film and the structure of QD-LEDs should be optimized

by selecting peripheral materials that match the AIS core/shell QDs.

2-4. Summary

The EL characteristics of QD-LEDs fabricated using AIS core/shell QDs with band-edge emission were investigated. EL emission mainly composed of band-edge emission was attained in the AIS-based QD-LED. However, the EL spectra of the QD-LEDs were found to involve a large defect emission component when compared with the PL spectra of the QD film. This defect emission was attributed to the electrons flowing in the EML being easily trapped at the defect levels in the QDs. Mixing 3TPYMB as CTMs into the EML effectively suppressed the defect emission. The addition of 3TPYMB also improved the electron injection into the QDs and the carrier balance in the EML. As a result, the defect emission was suppressed, and the EL characteristics were enhanced. It is expected that the method of improving the defect emission in EL will contribute to the development of high-color-purity QD-LEDs that do not contain toxic materials.

Chapter 3

QD-LEDs Exhibiting Narrow-Spectrum Green EL using Ag−In−Ga−S/GaS_x Core/shell QDs.

3-1. Introduction

For wide color gamut display applications of QD-LEDs, it is important to achieve high color purity for the three primary colors of RGB, particularly a narrow-spectrum green. AIGS core/shell QDs, in which a portion of In in the AIS core/shell QDs are replaced with Ga, are able to blue-shift narrow-spectrum emission and emit vivid green light. In 2018, Kameyama *et al.* achieved green-emitting AIGS core/shell QDs with a FWHM of 41 nm and a PLQY of 28%. The addition of a Ga source during the core synthesis of QDs shifted the emission wavelength of the QDs to the green region, compared to AIS core/shell QDs without Ga.[63] In 2021, Hoisang *et al.* synthesized Ag−In−Ga−S cores and GaS_x shells using gallium tris(diethyldithiocarbamate) ($Ga(DDTC)_3$) as raw material. The PLQY of green AIGS core/shell QDs was enhanced by forming thick shells using highly reactive raw materials.[64-65] In 2023, Uematsu *et al.* investigated the reaction mechanism of Ag–In–Ga–S cores and found that the formation yield of them can be increased by injecting an Ag source later in the synthesis process. They synthesized AIGS core/shell QDs with a very narrow emission with a FWHM of 31 nm.[67]

In addition to developments in QDs as emitting materials, improvements in layer structures of devices are also essential for enhancing the performance of QD-LEDs. Metal oxide materials such as ZnO NPs are commonly employed as charge injection layers due to their excellent charge injection into QDs. However, the luminescence degradation of QDs at the metal oxide interface remains a problem. The following approaches are being investigated to overcome this shortcoming: suppressing

the reactivity of ZnO NPs by metal doping or surface treatment,[91-93] using charge-injection materials instead of metal oxides,[70, 94] and inserting an interlayer between the QDs and the transport layer.[24, 39, 42]

In chapter 2, a yellow EL that composed mainly of band-edge emission from AIS core/shell QDs was successfully achieved by adding CTMs to the EML. In the initial stage of fabricating green AIGS QD-LEDs, AIGS core/shell QDs were applied to devices with the same structure as AIS QD-LEDs mixed with CTMs. Figure 3-1 shows the EL spectra of the AIGS QD-LED and the PL spectrum of the QD film. The EL spectra of the AIGS QD-LEDs without CTMs showed a strong defect emission component, with the intensity of the defect emission comparable to that of the band-edge emission. The addition of the CTMs reduced the defect emission component in the EL spectra of AIGS QD-LEDs. However, the defect emission was still higher than that in the PL spectrum of the AIGS QD film.[72] These results suggest that the addition of CTMs is not sufficient to improve the luminescence properties of AIGS QD-LEDs. It is necessary to eliminate specific defect-related emissions, which increase in EL, in order to utilize the remarkable color purity of AIGS QDs in QD-LEDs.

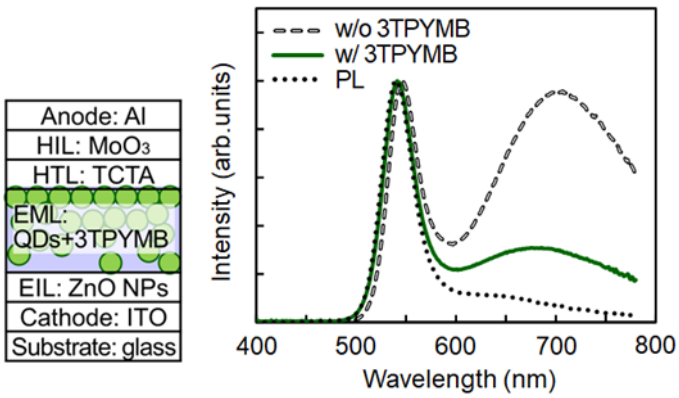


Figure 3-1. Structure of AIGS QD-LED with EML with 3TPYMB and EL spectra of the AIGS QD-LED with and without 3TPYMB, and PL spectra of QD film in the initial phase of the study.

In chapter 3, the fabrication of QD-LEDs using AIGS core/shell QDs that exhibit the band-edge emission and investigate their EL properties are reported. The added Ga compounds were effective in compensating for defect sites on the surface of the QDs, and the PLQY for the AIGS QD film was enhanced. The ZnMgO EIL was also treated with $GaCl_3$ to improve the luminescence properties of the QD-LEDs. In addition, CTMs with high electron transport properties were properly mixed with EML. As a result, the defect emission components in the EL were suppressed and the EL characteristics were improved. The EL exhibited a vibrant green color with color purity comparable to the PL of the AIGS QD film, regardless of the luminance.

3-2. Experimental section

3-2-1. Synthesis of AIGS core/shell QDs

The AIGS core/shell QDs used as a light-emitting material were synthesized by the following method.[67] In a 50-mL two-necked flask with a heating mantle, $InCl_3$ (0.2 mmol), $In(DDTC)_3$ (0.05 mmol), and $Ga(DDTC)_3$ (0.3 mmol) were mixed with OLA (10 mL) and heated at 80 °C under vacuum for 5 min. Once the powders were completely dissolved, the flask was filled with argon. Separately, Ag(OAc) (0.25 mmol) was dissolved in OLA (1 mL), and the solution was loaded into a gastight syringe. When the temperature of the In/Ga solution reached 130 °C, the Ag(OAc) solution was swiftly injected into the flask. After heating at 200 °C for 20 min, the solution was cooled to below 50 °C, and the nanoparticle portion was isolated by precipitation with acetone and methanol, and then dispersed in hexane (1 mL). To synthesize the GaS_x shell, 1 mL of $GaCl_3$ OLA solution (0.2 mmol/mL) and powdered $Ga(DDTC)_3$ (0.1 mmol, 52 mg) were mixed with OLA (9 mL) and evacuated at 80 °C. When the actual temperature reached 160 °C under an Ar atmosphere, the Ag-In-Ga-S core, dissolved in hexane, was injected dropwise, typically taking 1 min. The temperature was rapidly increased to 230 °C, and then to 280 °C at a rate of 2 °C min^{-1}. When the solution temperature reached 280 °C, 1 mL of the $GaCl_3$ OLA solution was injected. Heating was continued for another 30 min before cooling to room temperature. The resulting AIGS QDs were purified with methanol and ethanol and redispersed uniformly in chloroform.

3-2-2. Fabrication of AIGS QD-LEDs

The QD-LEDs were fabricated on glass substrates, onto which a 100-nm-thick indium tin oxide (ITO) was deposited and patterned as transparent electrodes. They were cleaned via sequential

sonication in a detergent solution and ethanol and treated in an ultraviolet-ozone cleaner. $Zn_{0.95}Mg_{0.05}O$ (ZnMgO) NPs were prepared according to the literature.[91] An EIL of ZnMgO NPs with a thickness of 40 nm was formed by spin-coating from the ethanol dispersion and baked at 180 °C. $GaCl_3$ was spin-coated on ZnMgO EIL from the chloroform solution at 0.05 mg mL^{-1} and baked at 210 °C. In the process of forming the EML, $GaCl_3$ and $Ga(DDTC)_3$ were added to the AIGS dispersions in chloroform, and 3TPYMB or 2,4,6-tris(3-(3-pyridyl)phenyl)-1,3,5-triazine (TmPPyTz),[95] as CTMs, was mixed into the dispersions. The QD dispersions for EMLs were spin-coated onto the EIL and baked at 100 °C. The thickness of the mixed EML was approximately 15 nm in total, including an approximately 10-nm QD part. On top of the EMLs, a 40-nm-thick HTL of TCTA, a 10-nm-thick HIL of MoO_3, and an 80-nm-thick Al anode were sequentially deposited by vacuum deposition. The QD-LEDs were encapsulated with a glass cover under a N_2 atmosphere.

3-2-3. Characterization

PL spectra of the emitting materials were recorded with a fluorescence and absorbance spectrometer (HORIBA, Duetta). PL quantum yield (QY) measurements were performed with a spectrofluorometer (Hamamatsu, PMA12). These PL measurements were excited with light at a wavelength of 400 nm. The luminance–current–voltage characteristics of the QD-LEDs were measured with a luminance meter (Konica Minolta, LS-110) and a source meter (Keithley, Model 2400), and their EL spectra were measured with a spectroradiometer (Konica Minolta, CS-2000A). The EQE was calculated from the current density, luminance, and EL spectrum under the assumption of Lambertian emission. Cross-sectional images of the QD-LEDs were observed with a scanning

electron microscope (Hitachi High-Tech, S-5500) after cross-sectional processing using a focused ion beam.

3-3. Results and discussion

3-3-1. PL characteristics of AIGS core/shell QDs

Figure 3-2-a shows the AIGS core/shell QD structure consisting of an Ag-In-Ga-S core, GaS_x shell, and oleylamine as a capping ligand protecting the surface. Figure 3-2-b and c show TEM images of the AIGS core NPs and AIGS core/shell QDs covered with GaS_x shell, respectively. The sizes of the cores and the core/shell QDs were 4.0 nm and 8.7 nm, respectively. The thickness of the GaS_x shell can be estimated 2.35 nm. Figure 3-2-d shows the PL spectra normalized by the peak intensity for the AIGS core/shell QDs as a dispersion in chloroform and as a spin-coated film. The dispersion exhibited green emission with a sharp peak at a wavelength of 529 nm and a weak broad component at wavelengths longer than 580 nm. The sharp peak derived from band-edge transitions implies that the GaS_x shell was effective in suppressing surface defects. The FWHM of the spectra observed from the AIGS QDs was 32 nm, which is extremely sharp for a low-toxicity QD, and the chromaticity coordinates of the green PL were (0.236, 0.709). The PLQY for the AIGS QDs after synthesis was 53%. AIGS QDs with a PLQY of 24% were used for QD-LEDs after several purifications to reduce

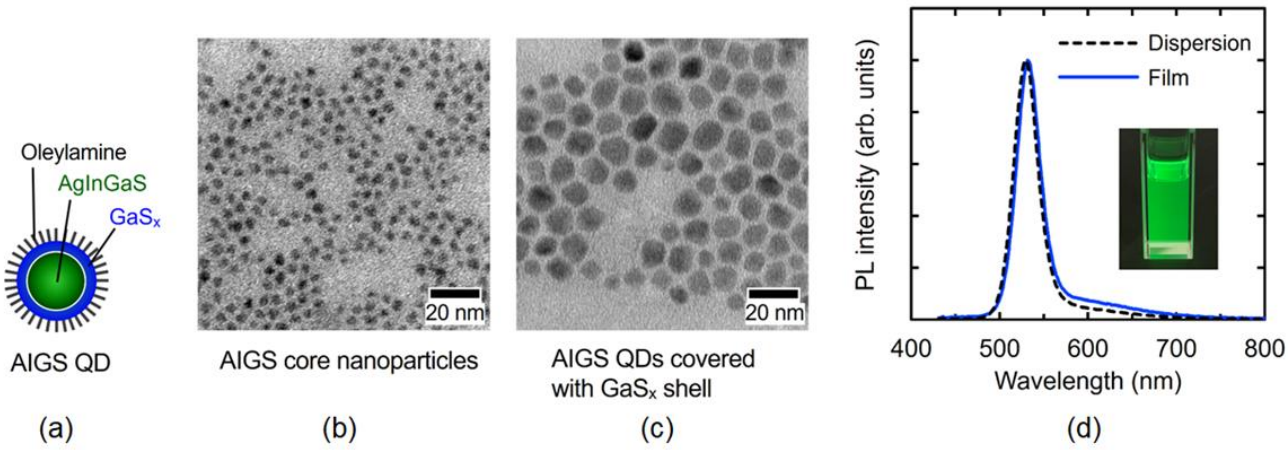


Figure 3-2. (a) Schematic of AIGS QD structure. TEM images of (b) AIGS core NPs and (c) those covered with a GaSx shell. (d) PL spectra of AIGS QDs in dispersion and in film. The PL spectra were normalized by the emission peak intensity, and the inset shows a photograph of the AIGS QD dispersion in chloroform.

the residual components. Purification was necessary to improve the QD film quality, but some useful ligands covering the shell were removed in the process, resulting in a decrease in the PLQY.

The AIGS QD film exhibited PL with a peak at a wavelength of 532 nm and an FWHM of 32 nm, and the PLQY was 16%. The PL spectra of the film tended to shift to longer wavelengths, as compared to the dispersion. Here, we calculated the radiation energy fraction for band-edge emission, which was estimated by fitting the peaks with a Gaussian function, in the total emission. The fraction of band-edge emission was 84% for the dispersion but decreased to 77% for the film. It is considered that the excitation energy for the film is more easily transferred to QDs with defect sites which have lower energy levels.

3-3-2. Improvement for mixed EML

To enhance the luminescence properties of AIGS QDs, The EMLs containing AIGS QDs, 3TPYMB as an ETM, and Ga compounds, namely $GaCl_3$ and $Ga(DDTC)_3$, were formed. Table 3-1 compares the PL characteristics of films fabricated under three different conditions: QD-only (EML1), QD+3TPYMB (EML2), and QD+3TPYMB+Ga compounds (EML3). The mixing ratios by weight were QD:3TPYMB = 1:1 (EML2) and QD:3TPYMB:Ga compounds = 1:1:0.1 (EML3). 3TPYMB had the effect of reducing the QD density in the EML, suppressing electron injection into defect sites

Table 3-1. PLQY and fraction of band-edge emission for mixed films at different ratios.

EML condition	Mixing ratio QD : 3TPYMB : Ga compounds	PL QY (%)	Fraction of band-edge emission (%) [a]
EML1	1 : 0 : 0	16	77
EML2	1 : 1 : 0	15	81
EML3	1 : 1 : 0.1	32	82

a) Fraction of between band-edge emission relative to total emission, as obtained by fitting the peaks with a Gaussian function.

in the QDs, and blocking holes in the EML. Although the PLQY for EML2 did not improve, the addition of 3TPYMB slightly suppressed the defect-related emission component in the spectra, and the fraction of band-edge emission increased to 81%. This is because the lower QD density in the mixed EML suppressed the energy crosstalk between QDs in the film, which typically increase low-energy emission. Meanwhile, the addition of Ga compounds to the EML lead to an increase in the PLQY. $Ga(DDTC)_3$, used in the synthesis of GaS_x shells as both a Ga and S source, is expected to form GaS_x to compensate for the shell via thermal decomposition of $Ga(DDTC)_3$ at relatively low temperatures.[65] $GaCl_3$, as a Z-type ligand, bonds to the S sites on the surface of the QD shell and passivates the dangling S sites.[66] These materials were added in the EML to cause reactions similar to shell synthesis and to protect the QD surface. The combination of $Ga(DDTC)_3$ and $GaCl_3$ increased the PLQY more effectively than either compound alone. In addition, these compounds improved PL without increasing defect-related emission. The PLQY was 32% and the fraction of band-edge emission was 82% in EML3.

Figure 3-3-a shows the structure of a QD-LED with an EML consisting of AIGS QDs. EMLs were compared for three different conditions: QD-only (EML1), QD+3TPYMB (EML2), and QD+3TPYMB+Ga compounds (EML3). The luminance–applied voltage curves and the EQE–current density characteristics for QD-LEDs are shown in Figures 3-3-b and c, respectively. The QD-LEDs with EML1 exhibited a low EQE owing to the QD EML condition. Some injected charge passed through to the counter electrode without being converted to light in the thin QD EML. Contact between AIGS QDs and a ZnMgO EIL was another cause of the weak luminescence. In contrast, the QD-LEDs with the mixed EML showed improved luminescence properties, owing to hole-blocking

and separation of the QD/ZnMgO interface that results from CTM deposition. In order to clarify the contact of QDs with ZnMgO, we measured the PLQY for QD films on ZnMgO layers.

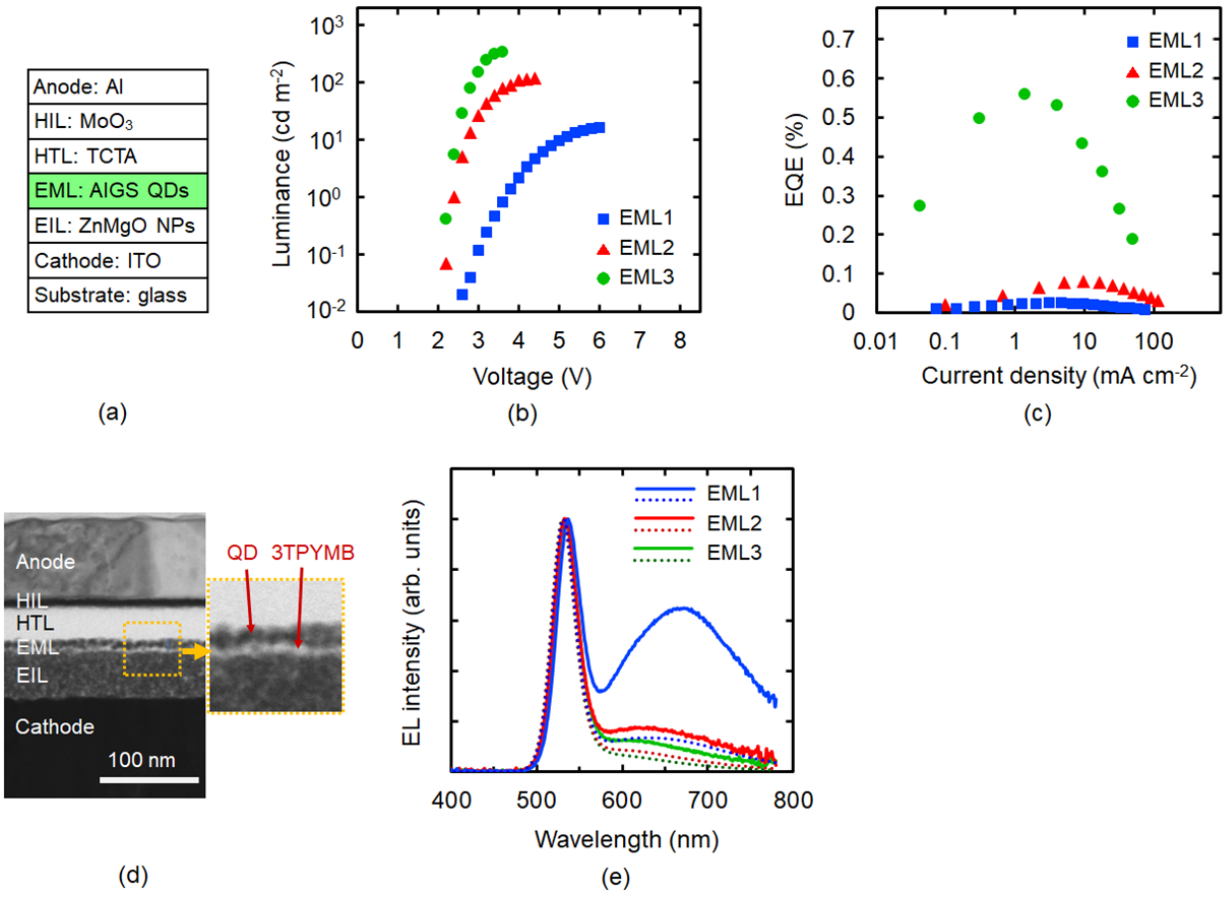


Figure 3-3. (a) Device structure of QD-LEDs. (b) Luminance–applied voltage and (c) EQE–current density plots for AIGS QD-LEDs with three different EML conditions. (d) Cross-sectional STEM image of QD-LED with EML3 and enlarged view of EML. (e) EL spectra of QD-LEDs with three different EML conditions for two values of luminance. The solid lines are the spectra at low luminance (0.01 cd m^{-2}), and the dotted lines are the spectra with the least defect-related emission (more than 10 cd m^{-2}).

Table 3-2. PLQY comparison of QD films on glass versus ZnMgO.

EML condition	PL QY (%)	
	On glass	On ZnMgO
EML1	16	8
EML2	15	14
EML3	32	30

Table 3-2 compares the PLQY for each QD film (EML1, EML2 and EML3) on glass versus ZnMgO. The PLQY for EML1 was lower on ZnMgO than on glass. The excitation energy from the QDs seems to be quenched at the interface between the QDs and ZnMgO. In contrast, the films mixed with 3TPYMB showed little decrease in PLQY. Figure 3-3-d shows a cross-sectional STEM image of a QD-LED with EML3. The mixed QDs and 3TPYMB were not uniformly dispersed in the EML but stacked separately in two layers. Most of the QDs were deposited in the upper part of the EML, leaving 3TPYMB on the bottom. The mixed 3TPYMB reduced the contact between the QDs and the ZnMgO EIL, and suppressed quenching at the interface. The added Ga compounds enhanced the luminescence properties of the EML, and the luminance and EQE of the QD-LEDs were increased by the mixed EMLs.

Figure 3-3-e shows EL spectra of the QD-LEDs, where the intensity was normalized with respect to the peak of the sharp band-edge emission. The spectra at low luminance (0.01 cd m^{-2}) for the three EMLs are shown with solid lines. The EL intensity in the wavelength region from 600 to 800 nm, which is strongly observed in EML1, is much more intense than that in the PL spectrum of the QD film in Figure 3-2-d. When the QDs were excited through the injection of electrons and holes under an electric field, the carriers were easily injected into the defect sites with low energy barriers, and the luminescence generated by defect sites was accentuated. EMLs formed by mixing QDs and 3TPYMB were able to suppress defect-related emission more effectively than the sequentially stacked QD/3TPYMB structure. Although the EL spectra at low luminance were improved by mixing 3TPYMB and Ga compounds, the defect-related emission component was still larger than in the case of PL. The defect-related emission components for each QD-LED were improved to the dotted lines in Figure 3e with increasing luminance (> 10 cd m^{-2}). The EL spectra of the QD-LEDs with EML3

were close to the PL spectrum. However, the fact that the spectra varied depending on the luminance remained a problem.

3-3-3. $GaCl_3$ treatment of ZnMgO EIL

In order to improve the EL spectra, the surface of the ZnMgO EIL was treated with $GaCl_3$. The deposited $GaCl_3$ did not only coat the EIL surface but also penetrated the EIL. Analysis of the EIL by X-ray photoelectron spectroscopy revealed the presence of Ga and Cl inside the EIL. The ZnMgO EIL was modified by chloride ions compensating for the oxygen deficiency in the ZnMgO NPs and by the generation of a gallium oxide component with good hole-blocking properties. The EL spectra of the QD-LEDs can be improved by suppressing direct injection into defect sites during electron injection from ZnMgO EIL into AIGS QDs.

Figure 3-4-a shows the luminance–applied voltage curves for QD-LEDs with mixed EMLs on EILs treated with $GaCl_3$. Since $GaCl_3$ treatment reduces electron injection into the AIGS QDs, the amount of $GaCl_3$ applied during the $GaCl_3$ treatment was adjusted so as to keep the turn-on voltage below 2.5

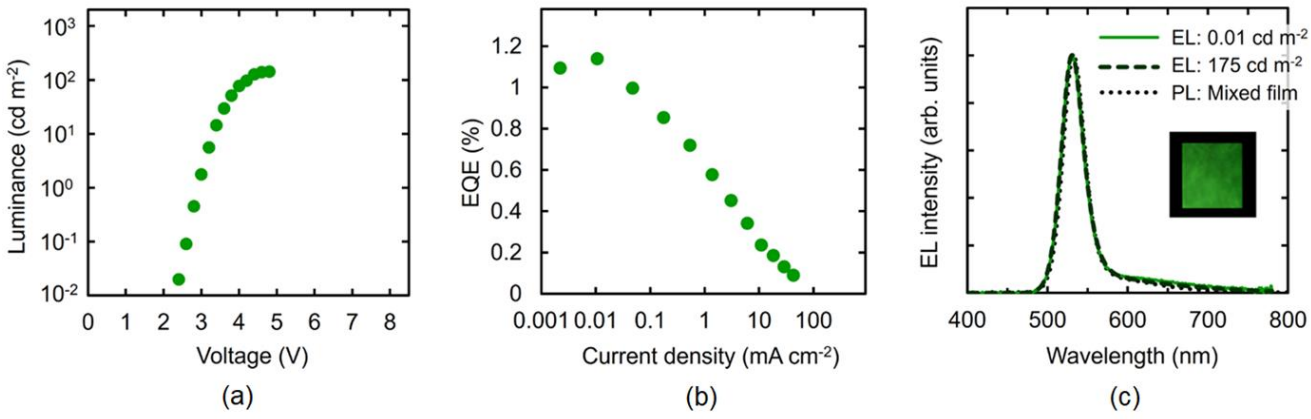


Figure 3-4. (a) Luminance−applied voltage and (b) EQE−current density plots for AIGS QD-LEDs with mixed EML on EILs treated with $GaCl_3$. (c) EL spectra of QD-LEDs at low (0.01 cd m^{-2}) and high luminance (175 cd m^{-2}) and PL spectrum of mixed QD film.

V. Figure 3-4-b shows the EQE–current density characteristics for the QD-LEDs. The EQE was improved to 1.1% by adjusting the interface between the EIL and the EML.

Figure 3-4-c shows EL spectra of QD-LEDs at low (0.01 cd m^{-2}) and high luminance (175 cd m^{-2}). Both had nearly the same shape as the PL spectra, the FWHM remained 33 nm, and almost no variation was observed in the EL spectra with luminance. The fraction of band-edge emission in the EL spectra was 81% at high luminance. The chromaticity of the QD-LEDs exhibited only a slight change from (0.268, 0.689) to (0.260, 0.695) over the luminance range from 0.01 to 175 cd m^{-2}, almost identical to the PL of the AIGS QD film (0.262, 0.697).

3-3-4. Application of highly transportable CTMs to QD-LEDs

The AIGS QD-LED mixed with 3TPYMB demonstrated remarkable defect emission suppression. However, reduced electron transport in 3TPYMB led to an increase in drive voltage and a decrease in luminescence properties in the high-luminance region. Therefore, 2,4,6-tris(3-(3-pyridyl)phenyl)-1,3,5-triazine (TmPPyTz), CTMs with excellent electron transport properties, was applied to the QD-LEDs to improve their luminescence properties.

Figure 3-5 shows a comparison of 3TPYMB and TmPPyTz as CTMs to be mixed in the EML of QD-LEDs. The QD-LEDs mixed with 3TPYMB require a higher driving voltage, and the EQEs decreased markedly in the region of higher luminance. In contrast, QD-LEDs mixed with TmPPyTz exhibited high luminance at lower voltages and maintained EQEs at higher luminance. The luminescence properties of the QD-LEDs showed a clear difference depending on the mixed CTMs, which was influenced by the deposition state of the EML. Figure 3-6 shows a cross-sectional STEM image of a QD-LED with 3TPYMB (a) and TmPPyTz (b). In the EML mixed with 3TPYMB, the

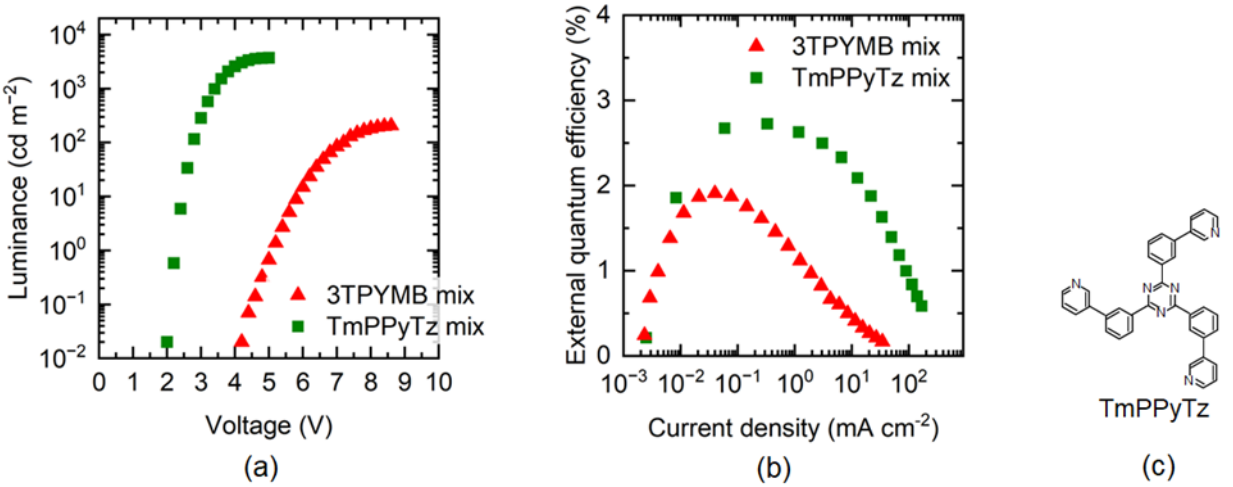


Figure 3-5. (a) Luminance−applied voltage and (b) EQE−current density plots for AIGS QD-LEDs with 3TPYMB and TmPPyTz. (c) Chemical structures of TmPPyTz.

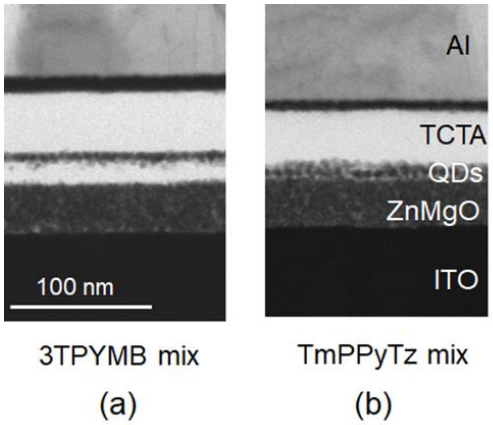


Figure 3-6. Cross-sectional STEM images of AIGS QD-LED with (a) 3TPYMB, and (b) TmPPyTz.

layers were deposited with a clear separation between QD and 3TPYMB, as mentioned in the previous section. In contrast, the EML mixed with TmPPyTz were not separated, and QDs and CTMs were deposited in an overall mixture. The presence of individual QDs is visible throughout the EML, indicating that TmPPyTz coordinates with the surface of the QDs and envelopes the particles. The enhanced charge injection properties from CTMs to QDs led to improve EL properties of QD-LEDs.

Figure 3-7 shows the EL characteristics of the AIGS QD-LEDs, which employed a blend of QDs, TmPPyTz, and 3TPYMB in the EML. Intriguingly, despite the incorporation of the lower condictivity 3TPYMB, the turn-on voltage was maintained low, and the EQE of the device was significantly improved to 5.4%. The cross-sectional STEM image (Figure 3-7c) reveals that the QDs were phase-separated within the EML, whereas the extent of separation was less than in the device using only

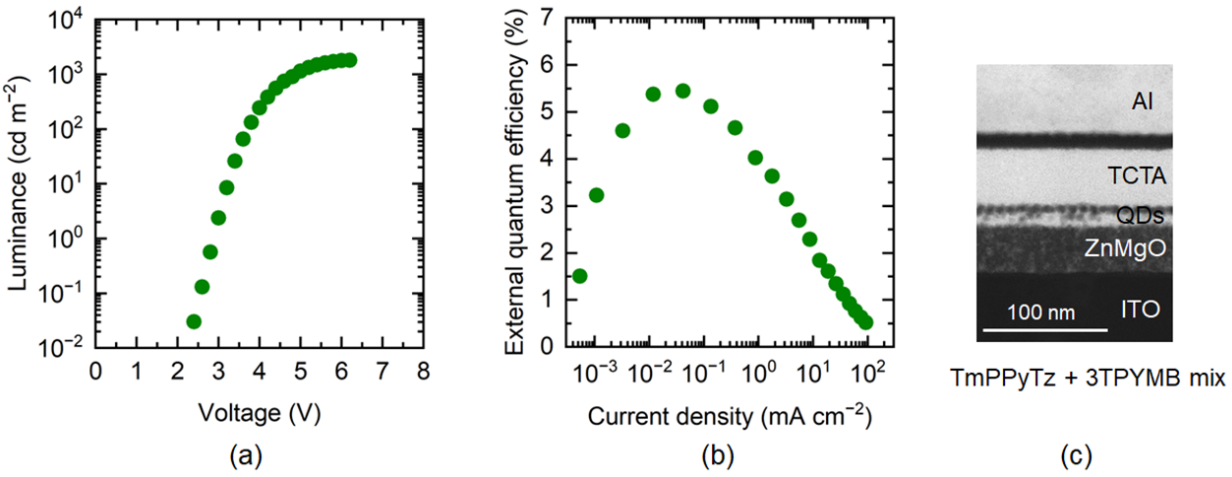


Figure 3-7. (a) Luminance−applied voltage and (b) EQE−current density plots for AIGS QD-LEDs with TmPPyTz and 3TPYMB, and (c) Cross-sectional STEM image of AIGS QD-LED with TmPPyTz and 3TPYMB.

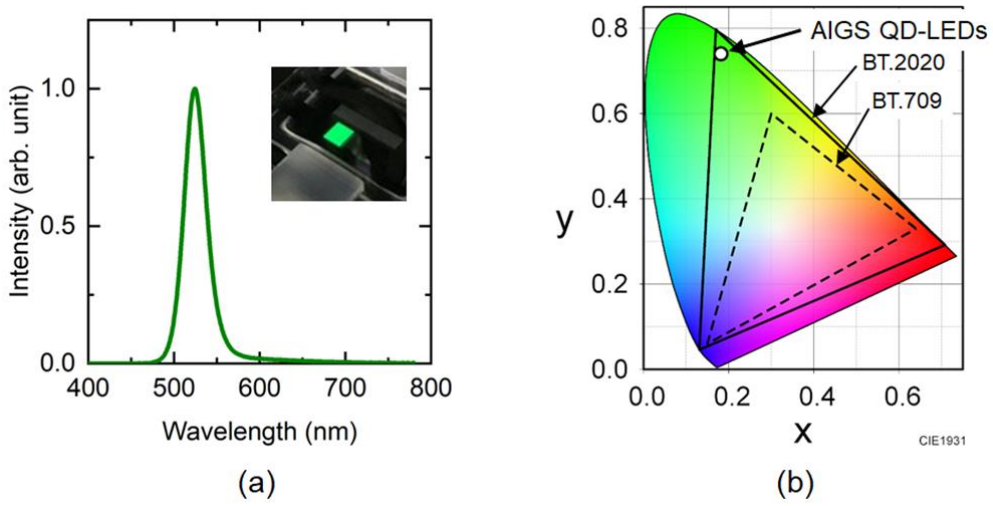


Figure 3-8. (a) EL spectra for AIGS QD-LEDs with TmPPyTz and 3TPYMB. (b) Chromaticity of AIGS QD-LEDs in CIE xy chromaticity diagram.

3TPYMB. This device structure could potentially offer benefits by employing 3TPYMB as a hole-blocking layer and simultaneously leveraging the charge injection properties of the well-miscible TmPPyTz.

Figure 3-8 shows the spectrum and chromaticity of the EL with the mixed CTMs, demonstrating a band-edge peak at 524 nm with an FWHM of 30 nm. Remarkably, the residual defect PL was almost completely eliminated, resulting in a chromaticity (0.182, 0.740) – indicative of extremely high color purity green EL. The fraction of the band-edge emission in the EL spectra reached 89%. It can be hypothesized that TmPPyTz contributed to the passivation of surface defects on the core/shell QDs through its pyridinic nitrogen.

3-4. Summary

The AIGS core/shell QDs, developed through a series of studies conducted by our research group, demonstrated vivid green PL with a good product yield. This was characterized by an intense, sharp band-edge peak with an FWHM of 32 nm. My research concentrated on the fabrication of QD-LEDs utilizing these AIGS core/shell QDs with a special emphasis on maintaining their monochromaticity even in the EL spectra.

The EL spectra of the AIGS QD-LEDs were found to involve a larger defect-related emission component than the PL spectra of the AIGS QD films. The defect emission was attributed to electrons that were injected into the EML, which were easily trapped at defect sites in the QDs. In order to address this issue, the AIGS QDs were treated with Ga compounds, such as $GaCl_3$ and $Ga(DDTC)_3$, which resulted in enhancing the luminescence properties of the EML. The Ga-based additives proved successful in passivating the defect sites on the surface of the QDs, resulting in the doubling of the PLQY from 16% to 32%. The ZnMgO layer, which serves as the EIL, was also treated with $GaCl_3$ for a similar modification. This aimed to further improve the luminescence properties of the QD-LEDs. As a consequence, it was confirmed that the monochromaticity of the EL was improved, primarily due to the suppression of direct electron injection from EIL to the defect sites within the AIGS QDs. Moreover, CTMs possessing excellent electron transport properties were meticulously mixed with EML, which improved the overall device performance.

As a result, the defect emission components in the EL were suppressed and the EL characteristics significantly enhanced, resulting in an improvement of the EQE to 5.4%. Importantly, the EL exhibited color purity comparable to the PL of the AIGS QD film, regardless of the luminance levels. The FWHM of the EL spectra observed from the QD-LEDs was found to be 30 nm, which is

remarkably narrow for the low-toxicity QD device. The chromaticity coordinates of the green EL were found to be (0.182, 0.740). It is expected that the proposed method for improving the EL characteristics will contribute to the development of high-color-purity displays with QD-LEDs that are free of toxic materials.

Conclusions

This dissertation described the design of a device structure aimed at the enhancement of the EL properties of QD-LEDs. This work specifically used multinary QDs composed of elements from groups 11, 13, and 16 to develop QD-LEDs with high color purity. While the devices using these multinary QDs have been successful in creating high color purity EL, primarily originating from band-edge transitions, the inherent crystal defects in these QDs have compromised color purity by introducing broad emission components that are stronger than those observed in PL. In this context, the focus was on optimizing the device structure by combining QDs with organic CTMs. The blend of QDs and CTMs in the EML not only improved the transport properties of the EML, but also suppressed defect emission components, thereby enhancing color purity.

In chapter 1, the fabrication process of QD-LEDs using low-toxicity ZAIS QDs was described in detail, followed by the evaluation of their EL properties. The synthesized ZAIS QDs produced a red PL with a peak wavelength of 700 nm. The relatively low charge injection barrier of the shell-free ZAIS QDs demonstrated the potential of the organic ETL to enhance the EL properties. By incorporating organic CTMs into the QD EML, it was possible to reduce the turn-on voltage to 2.4V and improved the EQE to 2.2%. The mixture EML composed of QDs and CTMs was effective in improving the overall characteristics of the QD-LEDs.

In chapter 2, the EL properties of AIS core/shell QDs with GaS_x shells, which exhibit yellow emission, were evaluated. The QD-LEDs using AIS core/shell QDs exhibited narrow-spectrum ELs mainly due to band-edge transitions. However, the EL spectra were found to contain a large defect emission component when compared with the PL spectra. This defect emission was attributed to the electrons flowing in the EML being easily trapped at the defect levels in the QDs. The addition of the

CTMs effectively suppressed the defect emission, resulting in color purity comparable to the PL of the QD film.

In chapter 3, the fabrication and analysis of QD-LEDs, which exhibit narrow-spectrum green EL utilizing AIGS core/shell QDs, are discussed. The EL spectra from these AIGS QD-LEDs contained large defect emission components. The measures described in Chapter 2 to blend CTMs were insufficient in fully improving the color purity of these QD-LEDs. Hence, an additional treatment with Ga compounds, along with the CTM mix, was applied to the QD-LEDs, which improved the color purity. Furthermore, CTMs with superior electron transport properties were meticulously mixed into the EML. This led to a notable improvement in EL characteristics and an EQE enhancement to 5.4%. The FWHM of the EL spectra from these QD-LEDs was 30 nm, an impressive value for a low-toxicity QD. Together with the suppressed defect EL, green emission was observed with high color purity at chromaticity coordinates (0.182, 0.740).

These methodological, stepwise approaches have succeeded in generating green EL from multinary QDs with an exceptionally high color purity. The achievement of such high color purity QD-LEDs using multinary QDs is a significant progress in the field. This progress is expected to pave the way for the development of display technologies that feature a wide color gamut.

References

1. Sugawara, M.; Choi, S.-Y.; Wood, D., Ultra-High-Definition Television (Rec. ITU-R BT.2020): A Generational Leap in the Evolution of Television. *IEEE Signal Process Mag.* **2014,** *31*, 170-174. DOI: 10.1109/msp.2014.2302331.
2. Parameter Values for Ultra-High Definition Television Systems for Production and International Programme Exchange; *Recommendation BT.2020-2*, International Telecommunication Union Radiocommunication Sector (ITU-R): 2015.
3. Masaoka, K.; Nishida, Y.; Sugawara, M., Designing Display Primaries with Currently Available Light Sources for Uhdtv Wide-Gamut System Colorimetry. *Opt. Express* **2014,** *22*, 19069-19077. DOI: 10.1364/OE.22.019069.
4. Ekimov, A. I.; Efros, A. L.; Onushchenko, A. A., Quantum Size Effect in Semiconductor Microcrystals. *Solid State Commun.* **1985,** *56*, 921-924. DOI: 10.1016/s0038-1098(85)80025-9.
5. Murray, C. B.; Norris, D. J.; Bawendi, M. G., Synthesis and Characterization of Nearly Monodisperse CdE (E = Sulfur, Selenium, Tellurium) Semiconductor Nanocrystallites. *J. Am. Chem. Soc.* **1993,** *115*, 8706-8715. DOI: 10.1021/ja00072a025.
6. Li, J.; Wang, L.-W., First Principle Study of Core/Shell Structure Quantum Dots. *Appl. Phys. Lett.* **2004,** *84*, 3648-3650. DOI: 10.1063/1.1737470.
7. Jang, E.; Jun, S.; Jang, H.; Lim, J.; Kim, B.; Kim, Y., White-Light-Emitting Diodes with Quantum Dot Color Converters for Display Backlights. *Adv. Mater.* **2010,** *22*, 3076-3080. DOI: 10.1002/adma.201000525.
8. Luo, Z.; Chen, Y.; Wu, S. T., Wide Color Gamut LCD with a Quantum Dot Backlight. *Opt. Express* **2013,** *21*, 26269-84. DOI: 10.1364/OE.21.026269.
9. Chen, H. W.; Zhu, R. D.; He, J.; Duan, W.; Hu, W.; Lu, Y. Q.; Li, M. C.; Lee, S. L.; Dong, Y. J.; Wu, S. T., Going Beyond the Limit of an LCD's Color Gamut. *Light Sci. Appl.* **2017,** *6*, e17043. DOI: 10.1038/lsa.2017.43.
10. Kim, H. M.; Ryu, M.; Cha, J. H. J.; Kim, H. S.; Jeong, T.; Jang, J., Ten Micrometer Pixel, Quantum Dots Color Conversion Layer for High Resolution and Full Color Active Matrix Micro‐LED Display. *J. Soc. Inf. Disp.* **2019,** *27*, 347-353. DOI: 10.1002/jsid.782.
11. Colvin, V. L.; Schlamp, M. C.; Alivisatos, A. P., Light-Emitting Diodes Made from Cadmium Selenide Nanocrystals and a Semiconducting Polymer. *Nature* **1994,** *370*, 354-357. DOI: 10.1038/370354a0.
12. Shirasaki, Y.; Supran, G. J.; Bawendi, M. G.; Bulović, V., Emergence of Colloidal Quantum-Dot Light-Emitting Technologies. *Nat. Photonics* **2012,** *7*, 13-23. DOI: 10.1038/nphoton.2012.328.
13. Davidson-Hall, T.; Aziz, H., Perspective: Toward Highly Stable Electroluminescent Quantum Dot Light-Emitting Devices in the Visible Range. *Appl. Phys. Lett.* **2020,** *116*, 010502. DOI: 10.1063/1.5134090.
14. Yuan, Q.; Wang, T.; Yu, P.; Zhang, H.; Zhang, H.; Ji, W., A Review on the Electroluminescence Properties of Quantum-Dot Light-Emitting Diodes. *Org. Electron.* **2021,** *90*, 106086. DOI: 10.1016/j.orgel.2021.106086.
15. Yang, J.; Choi, M. K.; Yang, U. J.; Kim, S. Y.; Kim, Y. S.; Kim, J. H.; Kim, D. H.; Hyeon, T., Toward Full-Color Electroluminescent Quantum Dot Displays. *Nano Lett.* **2021,** *21*, 26-33. DOI: 10.1021/acs.nanolett.0c03939.
16. Jeong, S. M.; Lim, T.; Park, J.; Han, C. Y.; Yang, H.; Ju, S., Pen Drawing Display. *Nat. Commun.* **2019,** *10*, 4334. DOI: 10.1038/s41467-019-12395-z.
17. Zhan, S.; Suh, Y. H.; Fan, X. B.; Yang, J.; Ni, L.; Kim, Y.; Jo, J. W.; Choi, H. W.; Jung, S. M.; Shin, D. W.; Lee, S.; Kim, J. M., Inkjet‐Printed Multi‐Color Arrays Based on Eco‐Friendly

Quantum Dot Light Emitting Diodes with Tailored Hole Transport Layer. *J. Soc. Inf. Disp.* **2022,** *30*, 748-757. DOI: 10.1002/jsid.1133.
18. Kim, T.-H.; Cho, K.-S.; Lee, E. K.; Lee, S. J.; Chae, J.; Kim, J. W.; Kim, D. H.; Kwon, J.-Y.; Amaratunga, G.; Lee, S. Y.; Choi, B. L.; Kuk, Y.; Kim, J. M.; Kim, K., Full-Colour Quantum Dot Displays Fabricated by Transfer Printing. *Nat. Photonics* **2011,** *5*, 176-182. DOI: 10.1038/nphoton.2011.12.
19. Meng, T.; Zheng, Y.; Zhao, D.; Hu, H.; Zhu, Y.; Xu, Z.; Ju, S.; Jing, J.; Chen, X.; Gao, H.; Yang, K.; Guo, T.; Li, F.; Fan, J.; Qian, L., Ultrahigh-Resolution Quantum-Dot Light-Emitting Diodes. *Nat. Photonics* **2022,** *16*, 297-303. DOI: 10.1038/s41566-022-00960-w.
20. Stouwdam, J. W.; Janssen, R. A. J., Red, Green, and Blue Quantum Dot Leds with Solution Processable ZnO Nanocrystal Electron Injection Layers. *J. Mater. Chem.* **2008,** *18*, 1889–1894. DOI: 10.1039/b800028j.
21. Qian, L.; Zheng, Y.; Xue, J.; Holloway, P. H., Stable and Efficient Quantum-Dot Light-Emitting Diodes Based on Solution-Processed Multilayer Structures. *Nat. Photonics* **2011,** *5*, 543-548. DOI: 10.1038/nphoton.2011.171.
22. Kwak, J.; Bae, W. K.; Lee, D.; Park, I.; Lim, J.; Park, M.; Cho, H.; Woo, H.; Yoon, D. Y.; Char, K.; Lee, S.; Lee, C., Bright and Efficient Full-Color Colloidal Quantum Dot Light-Emitting Diodes Using an Inverted Device Structure. *Nano Lett.* **2012,** *12*, 2362-2366. DOI: 10.1021/nl3003254.
23. Mashford, B. S.; Stevenson, M.; Popovic, Z.; Hamilton, C.; Zhou, Z.; Breen, C.; Steckel, J.; Bulovic, V.; Bawendi, M.; Coe-Sullivan, S.; Kazlas, P. T., High-Efficiency Quantum-Dot Light-Emitting Devices with Enhanced Charge Injection. *Nat. Photonics* **2013,** *7*, 407-412. DOI: 10.1038/nphoton.2013.70.
24. Dai, X.; Zhang, Z.; Jin, Y.; Niu, Y.; Cao, H.; Liang, X.; Chen, L.; Wang, J.; Peng, X., Solution-Processed, High-Performance Light-Emitting Diodes Based on Quantum Dots. *Nature* **2014,** *515*, 96-99. DOI: 10.1038/nature13829.
25. Yang, Y.; Zheng, Y.; Cao, W.; Titov, A.; Hyvonen, J.; Manders, J. R.; Xue, J.; Holloway, P. H.; Qian, L., High-Efficiency Light-Emitting Devices Based on Quantum Dots with Tailored Nanostructures. *Nat. Photonics* **2015,** *9*, 259-266. DOI: 10.1038/nphoton.2015.36.
26. Wang, L.; Lin, J.; Hu, Y.; Guo, X.; Lv, Y.; Tang, Z.; Zhao, J.; Fan, Y.; Zhang, N.; Wang, Y.; Liu, X., Blue Quantum Dot Light-Emitting Diodes with High Electroluminescent Efficiency. *ACS Appl. Mater. Interfaces* **2017,** *9*, 38755-38760. DOI: 10.1021/acsami.7b10785.
27. Cao, W.; Xiang, C.; Yang, Y.; Chen, Q.; Chen, L.; Yan, X.; Qian, L., Highly Stable QLEDs with Improved Hole Injection Via Quantum Dot Structure Tailoring. *Nat. Commun.* **2018,** *9*, 2608. DOI: 10.1038/s41467-018-04986-z.
28. Song, J.; Wang, O.; Shen, H.; Lin, Q.; Li, Z.; Wang, L.; Zhang, X.; Li, L. S., Over 30% External Quantum Efficiency Light‐Emitting Diodes by Engineering Quantum Dot‐Assisted Energy Level Match for Hole Transport Layer. *Adv. Funct. Mater.* **2019,** *29*, 1808377. DOI: 10.1002/adfm.201808377.
29. Lee, T.; Kim, B. J.; Lee, H.; Hahm, D.; Bae, W. K.; Lim, J.; Kwak, J., Bright and Stable Quantum Dot Light-Emitting Diodes. *Adv. Mater.* **2022,** *34*, 2106276. DOI: 10.1002/adma.202106276.
30. Chen, X.; Lin, X.; Zhou, L.; Sun, X.; Li, R.; Chen, M.; Yang, Y.; Hou, W.; Wu, L.; Cao, W.; Zhang, X.; Yan, X.; Chen, S., Blue Light-Emitting Diodes Based on Colloidal Quantum Dots with Reduced Surface-Bulk Coupling. *Nat. Commun.* **2023,** *14*, 284. DOI: 10.1038/s41467-023-35954-x.
31. Micic, O. I.; Curtis, C. J.; Jones, K. M.; Sprague, J. R.; Nozik, A. J., Synthesis and Characterization of InP Quantum Dots. *J. Phys. Chem.* **1994,** *98*, 4966-4969. DOI: 10.1021/j100070a004.
32. Xie, R.; Battaglia, D.; Peng, X., Colloidal InP Nanocrystals as Efficient Emitters Covering Blue

to near-Infrared. *J. Am. Chem. Soc.* **2007,** *129*, 15432-15433. DOI: 10.1021/ja076363h.
33. Tessier, M. D.; Dupont, D.; De Nolf, K.; De Roo, J.; Hens, Z., Economic and Size-Tunable Synthesis of InP/ZnE (E = S, Se) Colloidal Quantum Dots. *Chem. Mater.* **2015,** *27*, 4893-4898. DOI: 10.1021/acs.chemmater.5b02138.
34. Park, J. P.; Lee, J. J.; Kim, S. W., Highly Luminescent InP/GaP/ZnS QDs Emitting in the Entire Color Range via a Heating up Process. *Sci. Rep.* **2016,** *6*, 30094. DOI: 10.1038/srep30094.
35. Ramasamy, P.; Kim, N.; Kang, Y.-S.; Ramirez, O.; Lee, J.-S., Tunable, Bright, and Narrow-Band Luminescence from Colloidal Indium Phosphide Quantum Dots. *Chem. Mater.* **2017,** *29*, 6893-6899. DOI: 10.1021/acs.chemmater.7b02204.
36. Moriyama, T.; Kumamoto, A.; Kido, M.; Sasaki, H.; Novet, T.; Shibata, N.; Ikuhara, Y., Highly Luminescent and Narrow-Band-Emitting InP/ZnSe/ZnS Quantum Dot Synthesis by Halide Modified Shell Reaction. *Appl. Phys. Express* **2022,** *16*, 015504. DOI: 10.35848/1882-0786/aca9ba.
37. Lim, J.; Bae, W. K.; Lee, D.; Nam, M. K.; Jung, J.; Lee, C.; Char, K.; Lee, S., InP@ZnSeS, Core@Composition Gradient Shell Quantum Dots with Enhanced Stability. *Chem. Mater.* **2011,** *23*, 4459-4463. DOI: 10.1021/cm201550w.
38. Jiang, X.; Fan, Z.; Luo, L.; Wang, L., Advances and Challenges in Heavy-Metal-Free InP Quantum Dot Light-Emitting Diodes. *Micromachines* **2022,** *13*, 709. DOI: 10.3390/mi13050709.
39. Motomura, G.; Ogura, K.; Iwasaki, Y.; Nagakubo, J.; Hirakawa, M.; Nishihashi, T.; Tsuzuki, T., Improvement of Electroluminescent Characteristics in Quantum Dot Light-Emitting Diodes Using ZnInP/ZnSe/ZnS Quantum Dots by Mixing an Electron Transport Material into the Light-Emitting Layer. *AIP Adv.* **2020,** *10*, 065228. DOI: 10.1063/5.0010203.
40. Iwasaki, Y.; Motomura, G.; Ogura, K.; Tsuzuki, T., Efficient Green InP Quantum Dot Light-Emitting Diodes Using Suitable Organic Electron-Transporting Materials. *Appl. Phys. Lett.* **2020,** *117*, 111104. DOI: 10.1063/5.0020742.
41. Wu, Q.; Cao, F.; Wang, S.; Wang, Y.; Sun, Z.; Feng, J.; Liu, Y.; Wang, L.; Cao, Q.; Li, Y.; Wei, B.; Wong, W. Y.; Yang, X., Quasi-Shell-Growth Strategy Achieves Stable and Efficient Green InP Quantum Dot Light-Emitting Diodes. *Adv. Sci.* **2022,** *9*, e2200959. DOI: 10.1002/advs.202200959.
42. Lim, J.; Park, M.; Bae, W. K.; Lee, D.; Lee, S.; Lee, C.; Char, K., Highly Efficient Cadmium-Free Quantum Dot Light-Emitting Diodes Enabled by the Direct Formation of Excitons within InP@ZnSeS Quantum Dots. *ACS Nano* **2013,** *7*, 9019-9026. DOI: 10.1021/nn403594j.
43. Cao, F.; Wang, S.; Wang, F.; Wu, Q.; Zhao, D.; Yang, X., A Layer-by-Layer Growth Strategy for Large-Size InP/ZnSe/ZnS Core–Shell Quantum Dots Enabling High-Efficiency Light-Emitting Diodes. *Chem. Mater.* **2018,** *30*, 8002-8007. DOI: 10.1021/acs.chemmater.8b03671.
44. Won, Y. H.; Cho, O.; Kim, T.; Chung, D. Y.; Kim, T.; Chung, H.; Jang, H.; Lee, J.; Kim, D.; Jang, E., Highly Efficient and Stable InP/ZnSe/ZnS Quantum Dot Light-Emitting Diodes. *Nature* **2019,** *575*, 634-638. DOI: 10.1038/s41586-019-1771-5.
45. Bang, J.; Park, J.; Lee, J. H.; Won, N.; Nam, J.; Lim, J.; Chang, B. Y.; Lee, H. J.; Chon, B.; Shin, J.; Park, J. B.; Choi, J. H.; Cho, K.; Park, S. M.; Joo, T.; Kim, S., ZnTe/ZnSe (Core/Shell) Type-II Quantum Dots: Their Optical and Photovoltaic Properties. *Chem. Mater.* **2009,** *22*, 233-240. DOI: 10.1021/cm9027995.
46. Wang, A.; Shen, H.; Zang, S.; Lin, Q.; Wang, H.; Qian, L.; Niu, J.; Song Li, L., Bright, Efficient, and Color-Stable Violet ZnSe-Based Quantum Dot Light-Emitting Diodes. *Nanoscale* **2015,** *7*, 2951-2959. DOI: 10.1039/c4nr06593j.
47. Asano, H.; Arai, K.; Kita, M.; Omata, T., Synthesis of Colloidal Zn(Te,Se) Alloy Quantum Dots. *Mater. Res. Express* **2017,** *4*, 106501. DOI: 10.1088/2053-1591/aa8b84.
48. Han, C.-Y.; Lee, S.-H.; Song, S.-W.; Yoon, S.-Y.; Jo, J.-H.; Jo, D.-Y.; Kim, H.-M.; Lee, B.-J.; Kim, H.-S.; Yang, H., More Than 9% Efficient ZnSeTe Quantum Dot-Based Blue

Electroluminescent Devices. *ACS Energy Lett.* **2020,** *5*, 1568-1576. DOI: 10.1021/acsenergylett.0c00638.
49. Ryowa, T.; Ishida, T.; Sakakibara, Y.; Kitano, K.; Ueda, M.; Izumi, M.; Ogura, Y.; Tanaka, M.; Nikata, S.; Watanabe, M.; Takasaki, M.; Itoh, T.; Miyanaga, A., High‐Efficiency Quantum Dot Light‐Emitting Diodes with Blue Cadmium‐Free Quantum Dots. *J. Soc. Info. Disp.* **2020,** *28*, 401-409. DOI: 10.1002/jsid.896.
50. Kim, T.; Kim, K. H.; Kim, S.; Choi, S. M.; Jang, H.; Seo, H. K.; Lee, H.; Chung, D. Y.; Jang, E., Efficient and Stable Blue Quantum Dot Light-Emitting Diode. *Nature* **2020,** *586*, 385-389. DOI: 10.1038/s41586-020-2791-x.
51. Lee, S.-H.; Han, C.-Y.; Song, S.-W.; Jo, D.-Y.; Jo, J.-H.; Yoon, S.-Y.; Kim, H.-M.; Hong, S.; Hwang, J. Y.; Yang, H., Znsete Quantum Dots as an Alternative to Inp and Their High-Efficiency Electroluminescence. *Chem. Mater.* **2020,** *32*, 5768-5775. DOI: 10.1021/acs.chemmater.0c01596.
52. Torimoto, T.; Adachi, T.; Okazaki, K.; Sakuraoka, M.; Shibayama, T.; Ohtani, B.; Kudo, A.; Kuwabata, S., Facile Synthesis of ZnS-$AgInS_2$ Solid Solution Nanoparticles for a Color-Adjustable Luminophore. *J. Am. Chem. Soc.* **2007,** *129*, 12388-12389. DOI: 10.1021/ja0750470.
53. Castro, S. L.; Bailey, S. G.; Raffaelle, R. P.; Banger, K. K.; Hepp, A. F., Synthesis and Characterization of Colloidal $CuInS_2$ Nanoparticles from a Molecular Single-Source Precursor. *J. Phys. Chem. B* **2004,** *108*, 12429-12435. DOI: 10.1021/jp049107p.
54. Nakamura, H.; Kato, W.; Uehara, M.; Nose, K.; Omata, T.; Otsuka-Yao-Matsuo, S.; Miyazaki, M.; Maeda, H., Tunable Photoluminescence Wavelength of Chalcopyrite $CuInS_2$-Based Semiconductor Nanocrystals Synthesized in a Colloidal System. *Chem. Mater.* **2006,** *18*, 3330-3335. DOI: 10.1021/cm0518022.
55. Uehara, M.; Watanabe, K.; Tajiri, Y.; Nakamura, H.; Maeda, H., Synthesis of $CuInS_2$ Fluorescent Nanocrystals and Enhancement of Fluorescence by Controlling Crystal Defect. *J Chem Phys* **2008,** *129*, 134709. DOI: 10.1063/1.2987707.
56. Uematsu, T.; Doi, T.; Torimoto, T.; Kuwabata, S., Preparation of Luminescent $AgInS_2$−$AgGaS_2$ Solid Solution Nanoparticles and Their Optical Properties. *J. Phys. Chem. Lett.* **2010,** *1*, 3283-3287. DOI: 10.1021/jz101295w.
57. Tan, Z.; Zhang, Y.; Xie, C.; Su, H.; Liu, J.; Zhang, C.; Dellas, N.; Mohney, S. E.; Wang, Y.; Wang, J.; Xu, J., Near-Band-Edge Electroluminescence from Heavy-Metal-Free Colloidal Quantum Dots. *Adv. Mater.* **2011,** *23*, 3553-3558. DOI: 10.1002/adma.201100719.
58. Zhong, H.; Wang, Z.; Bovero, E.; Lu, Z.; van Veggel, F. C. J. M.; Scholes, G. D., Colloidal Cuinse2 Nanocrystals in the Quantum Confinement Regime: Synthesis, Optical Properties, and Electroluminescence. *J. Phys. Chem. C* **2011,** *115*, 12396-12402. DOI: 10.1021/jp204249j.
59. Xie, X.; Zhao, J.; Lin, O.; Yin, Z.; Li, X.; Zhang, Y.; Tang, A., Narrow-Bandwidth Blue-Emitting Ag-Ga-Zn-S Semiconductor Nanocrystals for Quantum-Dot Light-Emitting Diodes. *J. Phys. Chem. Lett.* **2022,** *13*, 11857-11863. DOI: 10.1021/acs.jpclett.2c03437.
60. Lu, H.; Hu, Z.; Zhou, W.; Wei, J.; Zhang, W.; Xie, F.; Guo, R., Synthesis and Structure Design of I–III–VI Quantum Dots for White Light-Emitting Diodes. *Mater. Chem. Front.* **2022,** *6*, 418-429. DOI: 10.1039/d1qm01452h.
61. Yang, L.; Zhang, S.; Xu, B.; Jiang, J.; Cai, B.; Lv, X.; Zou, Y.; Fan, Z.; Yang, H.; Zeng, H., I-III-VI Quantum Dots and Derivatives: Design, Synthesis, and Properties for Light-Emitting Diodes. *Nano Lett.* **2023,** *23*, 2443-2453. DOI: 10.1021/acs.nanolett.2c03138.
62. Uematsu, T.; Wajima, K.; Sharma, D. K.; Hirata, S.; Yamamoto, T.; Kameyama, T.; Vacha, M.; Torimoto, T.; Kuwabata, S., Narrow Band-Edge Photoluminescence from $AgInS_2$ Semiconductor Nanoparticles by the Formation of Amorphous III–VI Semiconductor Shells. *NPG Asia Mater.* **2018,** *10*, 713-726. DOI: 10.1038/s41427-018-0067-9.
63. Kameyama, T.; Kishi, M.; Miyamae, C.; Sharma, D. K.; Hirata, S.; Yamamoto, T.; Uematsu, T.;

Vacha, M.; Kuwabata, S.; Torimoto, T., Wavelength-Tunable Band-Edge Photoluminescence of Nonstoichiometric Ag–In–S Nanoparticles Via Ga^{3+} Doping. *ACS Appl. Mater. Interfaces* **2018,** *10*, 42844-42855. DOI: 10.1021/acsami.8b15222.

64. Hoisang, W.; Uematsu, T.; Torimoto, T.; Kuwabata, S., Photoluminescence Stability Enhancement of Ag–In–Ga–S/GaS_x Core/Shell Quantum Dots with Thicker Shells by the Addition of Gallium Diethyldithiocarbamate. *Chem. Lett.* **2021,** *50*, 1863-1866. DOI: 10.1246/cl.210363.
65. Hoisang, W.; Uematsu, T.; Torimoto, T.; Kuwabata, S., Luminescent Quaternary Ag(In_xGa_{1-x})S_2/GaS_y Core/Shell Quantum Dots Prepared Using Dithiocarbamate Compounds and Photoluminescence Recovery Via Post Treatment. *Inorg Chem* **2021,** *60*, 13101-13109. DOI: 10.1021/acs.inorgchem.1c01513.
66. Hoisang, W.; Uematsu, T.; Torimoto, T.; Kuwabata, S., Surface Ligand Chemistry on Quaternary Ag(In_xGa_{1-x})S_2 Semiconductor Quantum Dots for Improving Photoluminescence Properties. *Nanoscale Adv.* **2022,** *4*, 849-857. DOI: 10.1039/d1na00684c.
67. Uematsu, T.; Tepakidareekul, M.; Hirano, T.; Torimoto, T.; Kuwabata, S., Facile High-Yield Synthesis of Ag–In–Ga–S Quaternary Quantum Dots and Coating with Gallium Sulfide Shells for Narrow Band-Edge Emission. *Chem. Mater.* **2023,** *35*, 1094-1106. DOI: 10.1021/acs.chemmater.2c03023.
68. Kameyama, T.; Yamauchi, H.; Yamamoto, T.; Mizumaki, T.; Yukawa, H.; Yamamoto, M.; Ikeda, S.; Uematsu, T.; Baba, Y.; Kuwabata, S.; Torimoto, T., Tailored Photoluminescence Properties of Ag(In,Ga)Se_2 Quantum Dots for near-Infrared in Vivo Imaging. *ACS Appl. Nano Mater.* **2020,** *3*, 3275-3287. DOI: 10.1021/acsanm.9b02608.
69. Jiang, C.; Tozawa, M.; Akiyoshi, K.; Kameyama, T.; Yamamoto, T.; Motomura, G.; Fujisaki, Y.; Uematsu, T.; Kuwabata, S.; Torimoto, T., Development of Cu-In-Ga-S Quantum Dots with a Narrow Emission Peak for Red Electroluminescence. *J. Chem. Phys.* **2023,** *158*, 164708. DOI: 10.1063/5.0144271.
70. Motomura, G.; Ogura, K.; Kameyama, T.; Torimoto, T.; Uematsu, T.; Kuwabata, S.; Tsuzuki, T., Efficient Quantum-Dot Light-Emitting Diodes Using ZnS–$AgInS_2$ Solid-Solution Quantum Dots in Combination with Organic Charge-Transport Materials. *Appl. Phys. Lett.* **2020,** *116*, 093302. DOI: 10.1063/1.5143618.
71. Motomura, G.; Ogura, K.; Iwasaki, Y.; Uematsu, T.; Kuwabata, S.; Kameyama, T.; Torimoto, T.; Tsuzuki, T., Electroluminescence from Band-Edge-Emitting $AgInS_2$/GaS_x Core/Shell Quantum Dots. *Appl. Phys. Lett.* **2020,** *117*, 091101. DOI: 10.1063/5.0018132.
72. Motomura, G.; Iwasaki, Y.; Kameyama, T.; Torimoto, T.; Uematsu, T.; Kuwabata, S.; Tsuzuki, T., Green Electroluminescence Generated by Band-Edge Transition in Ag-In-Ga-S/GaS_x Core/Shell Quantum Dots. *ITE Trans. on MTA* **2021,** *9*, 222-227. DOI: 10.3169/mta.9.222.
73. Motomura, G.; Uematsu, T.; Kuwabata, S.; Kameyama, T.; Torimoto, T.; Tsuzuki, T., Quantum-Dot Light-Emitting Diodes Exhibiting Narrow-Spectrum Green Electroluminescence by Using Ag–In–Ga–S/GaS_x Quantum Dots. *ACS Appl. Mater. Interfaces* **2023,** *15*, 8336-8344. DOI: 10.1021/acsami.2c21232.
74. Kameyama, T.; Takahashi, T.; Machida, T.; Kamiya, Y.; Yamamoto, T.; Kuwabata, S.; Torimoto, T., Controlling the Electronic Energy Structure of ZnS–$AgInS_2$ Solid Solution Nanocrystals for Photoluminescence and Photocatalytic Hydrogen Evolution. *J. Phys. Chem. C* **2015,** *119*, 24740-24749. DOI: 10.1021/acs.jpcc.5b07994.
75. Bhaumik, S.; Guchhait, A.; Pal, A. J., Light-Emitting Diodes Based on Nontoxic Zinc-Alloyed Silver–Indium-Sulfide (AIZS) Nanocrystals. *Physica E* **2014,** *58*, 124-129. DOI: 10.1016/j.physe.2013.12.007.
76. Zhu, B.; Ji, W.; Duan, Z.; Sheng, Y.; Wang, T.; Yuan, Q.; Zhang, H.; Tang, X.; Zhang, H., Low Turn-on Voltage and Highly Bright Ag–In–Zn–S Quantum Dot Light-Emitting Diodes. *J. Mater.*

Chem. C **2018,** *6*, 4683-4690. DOI: 10.1039/c8tc01022f.
77. Kim, J.-H.; Yang, H., High-Efficiency Cu–In–S Quantum-Dot-Light-Emitting Device Exceeding 7%. *Chem. Mater.* **2016,** *28*, 6329-6335. DOI: 10.1021/acs.chemmater.6b02669.
78. Gao, Z.; Lee, C. S.; Bello, I.; Lee, S. T.; Chen, R.-M.; Luh, T.-Y.; Shi, J.; Tang, C. W., Bright-Blue Electroluminescence from a Silyl-Substituted Ter-(Phenylene–Vinylene) Derivative. *Appl. Phys. Lett.* **1999,** *74*, 865-867. DOI: 10.1063/1.123392.
79. Tsuzuki, T.; Motomura, G.; Yamamoto, T., Quantum Dot Light-Emitting Diode Using 2,2′-Bis(N-Carbazolyl)-9,9′-Spirobifluorene as a Morphologically and Thermally Stable Hole-Transporting Material. *Phys. Status Solidi A* **2016,** *213*, 3194-3198. DOI: 10.1002/pssa.201600270.
80. Coe-Sullivan, S.; Steckel, J. S.; Woo, W. K.; Bawendi, M. G.; Bulović, V., Large-Area Ordered Quantum-Dot Monolayers Via Phase Separation During Spin-Casting. *Adv. Funct. Mater.* **2005,** *15*, 1117-1124. DOI: 10.1002/adfm.200400468.
81. Iwasaki, Y.; Motomura, G.; Tsuzuki, T., Pure-Colored Red, Green, and Blue Quantum Dot Light-Emitting Diodes Using Emitting Layers Composed of Cadmium-Free Quantum Dots and Organic Electron-Transporting Materials. *Jpn. J. Appl. Phys.* **2022,** *61*, 052004. DOI: 10.35848/1347-4065/ac54fa.
82. Anikeeva, P. O.; Halpert, J. E.; Bawendi, M. G.; Bulovic, V., Quantum Dot Light-Emitting Devices with Electroluminescence Tunable over the Entire Visible Spectrum. *Nano Lett.* **2009,** *9*, 2532-2536. DOI: 10.1021/nl9002969.
83. Chang, Y.-T.; Liu, S.-W.; Yuan, C.-H.; Ho, Y.-H.; Chen, K.-Y.; Lee, Y.-T.; Wu, M.-F.; Lee, C.-C.; Wei, P.-K.; Chen, C.-T.; Wu, C.-I., Comparison of Light out-Coupling Enhancements in Single-Layer Blue-Phosphorescent Organic Light Emitting Diodes Using Small-Molecule or Polymer Hosts. *J. Appl. Phys.* **2013,** *114*, 173106. DOI: 10.1063/1.4829677.
84. Jimenez-Lopez, J.; Cambarau, W.; Cabau, L.; Palomares, E., Charge Injection, Carriers Recombination and Homo Energy Level Relationship in Perovskite Solar Cells. *Sci. Rep.* **2017,** *7*, 6101. DOI: 10.1038/s41598-017-06245-5.
85. Hoisang, W.; Uematsu, T.; Yamamoto, T.; Torimoto, T.; Kuwabata, S., Core Nanoparticle Engineering for Narrower and More Intense Band-Edge Emission from $AgInS_2/GaS_x$ Core/Shell Quantum Dots. *Nanomaterials* **2019,** *9*, 1763. DOI: 10.3390/nano9121763.
86. Ji, W.; Jing, P.; Zhang, L.; Li, D.; Zeng, Q.; Qu, S.; Zhao, J., The Work Mechanism and Sub-Bandgap-Voltage Electroluminescence in Inverted Quantum Dot Light-Emitting Diodes. *Sci. Rep.* **2014,** *4*, 6974. DOI: 10.1038/srep06974.
87. Sun, Y.; Jiang, Y.; Peng, H.; Wei, J.; Zhang, S.; Chen, S., Efficient Quantum Dot Light-Emitting Diodes with a $Zn_{0.85}Mg_{0.15}O$ Interfacial Modification Layer. *Nanoscale* **2017,** *9*, 8962-8969. DOI: 10.1039/c7nr02099f.
88. Tanaka, D.; Takeda, T.; Chiba, T.; Watanabe, S.; Kido, J., Novel Electron-Transport Material Containing Boron Atom with a High Triplet Excited Energy Level. *Chem. Lett.* **2007,** *36*, 262-263. DOI: 10.1246/cl.2007.262.
89. Kim, S.-K.; Kim, Y.-S., Charge Carrier Injection and Transport in QLED Layer with Dynamic Equilibrium of Trapping/De-Trapping Carriers. *J. Appl. Phys.* **2019,** *126*, 035704. DOI: 10.1063/1.5109089.
90. Cocchi, M.; Kalinowski, J.; Fattori, V.; Williams, J. A. G.; Murphy, L., Color-Variable Highly Efficient Organic Electrophosphorescent Diodes Manipulating Molecular Exciton and Excimer Emissions. *Appl. Phys. Lett.* **2009,** *94*, 073309. DOI: 10.1063/1.3086900.
91. Kim, J.-H.; Han, C.-Y.; Lee, K.-H.; An, K.-S.; Song, W.; Kim, J.; Oh, M. S.; Do, Y. R.; Yang, H., Performance Improvement of Quantum Dot-Light-Emitting Diodes Enabled by an Alloyed ZnMgO Nanoparticle Electron Transport Layer. *Chem. Mater.* **2015,** *27*, 197-204. DOI: 10.1021/cm503756q.

92. Chen, F.; Liu, Z.; Guan, Z.; Liu, Z.; Li, X.; Deng, Z.; Teng, F.; Tang, A., Chloride-Passivated Mg-Doped ZnO Nanoparticles for Improving Performance of Cadmium-Free, Quantum-Dot Light-Emitting Diodes. *ACS Photonics* **2018,** *5*, 3704-3711. DOI: 10.1021/acsphotonics.8b00722.
93. Sun, Z.; Wu, Q.; Wang, S.; Cao, F.; Wang, Y.; Li, L.; Wang, H.; Kong, L.; Yan, L.; Yang, X., Suppressing the Cation Exchange at the Core/Shell Interface of InP Quantum Dots by a Selenium Shielding Layer Enables Efficient Green Light-Emitting Diodes. *ACS Appl. Mater. Interfaces* **2022,** *14*, 15401-15406. DOI: 10.1021/acsami.2c01699.
94. Cao, F.; Wu, Q.; Sui, Y.; Wang, S.; Dou, Y.; Hua, W.; Kong, L.; Wang, L.; Zhang, J.; Jiang, T.; Yang, X., All-Inorganic Quantum Dot Light-Emitting Diodes with Suppressed Luminance Quenching Enabled by Chloride Passivated Tungsten Phosphate Hole Transport Layers. *Small* **2021,** *17*, e2100030. DOI: 10.1002/smll.202100030.
95. Su, S. J.; Sasabe, H.; Pu, Y. J.; Nakayama, K.; Kido, J., Tuning Energy Levels of Electron-Transport Materials by Nitrogen Orientation for Electrophosphorescent Devices with an 'Ideal' Operating Voltage. *Adv. Mater.* **2010,** *22*, 3311-3316. DOI: 10.1002/adma.200904249.

Acknowledgements

The author would like to express his sincerest gratitude to Prof. Dr. Susumu Kuwabata at Department of Applied Chemistry, Graduate School of Engineering, Osaka University who provided continuous guidance, and valuable suggestions throughout this work. The author would like to thank Prof. Dr. Nobuhito Imanaka and Prof. Dr. Akinori Saeki, at Department of Applied Chemistry, Graduate School of Engineering, Osaka University for their careful reviews and valuable suggestions.

The author also would like to express his special thanks to Associate Prof. Dr. Taro Uematsu at Department of Applied Chemistry, Graduate School of Engineering, Osaka University, who provide enthusiastic guidance, invaluable feedback, and fruitful discussion throughout this work. The author is also grateful to all members of Kuwabata Laboratory for their invaluable support.

The author would like to express his deeply appreciation to Dr. Toru Imai, Director of NHK STRL, and Dr. Norihiko Ishii, Head of Advance Functional devices Research Division, NHK STRL, for allowing me to conduct research at the graduate school. The author is deeply grateful to Dr. Toshimitsu Tsuzuki and Dr. Yoshihide Fujisaki at NHK STRL, for their helpful support and kind feedback throughout research activity. The author is also grateful to all the members who worked on this research at NHK STRL.

The author is deeply grateful to Prof. Dr. Tsukasa Torimoto and Associate Prof. Dr. Tatsuya Kameyama at Department of Materials Chemistry, Graduate School of Engineering, Nagoya University, for their accurate guidance and valuable discussion. The author is also grateful to all members of Torimoto Laboratory for their invaluable support.

Finally, the author would like to express his sincere gratitude to his wife Ryoko Motomura for her hearty support and warm encouragements.

Genichi Motomura
June, 2023